Kindlin-3–mediated signaling from multiple integrin classes is required for osteoclast-mediated bone resorption

Sarah Schmidt,[1] Inaam Nakchbandi,[1,2] Raphael Ruppert,[1] Nina Kawelke,[1,2] Michael W. Hess,[3] Kristian Pfaller,[3] Pierre Jurdic,[4] Reinhard Fässler,[1] and Markus Moser[1]

[1]Max Planck Institute of Biochemistry, D-82152 Martinsried, Germany
[2]University of Heidelberg, D-69120 Heidelberg, Germany
[3]Innsbruck Medical University, Division of Histology and Embryology, A-6020 Innsbruck, Austria
[4]University of Lyon, Ecole Normale Supérieure de Lyon, 69364 Lyon, France

The blood cell–specific kindlin-3 protein is required to activate leukocyte and platelet integrins. In line with this function, mutations in the *KINDLIN-3* gene in man cause immunodeficiency and severe bleeding. Some patients also suffer from osteopetrosis, but the underlying mechanism leading to abnormal bone turnover is unknown. Here we show that kindlin-3–deficient mice develop severe osteopetrosis because of profound adhesion and spreading defects in bone-resorbing osteoclasts. Mechanistically, loss of kindlin-3 impairs the activation of β1, β2, and β3 integrin classes expressed on osteoclasts, which in turn abrogates the formation of podosomes and sealing zones required for bone resorption. In agreement with these findings, genetic ablation of all integrin classes abolishes the development of podosomes, mimicking kindlin-3 deficiency. Although loss of single integrin classes gives rise to podosomes, their resorptive activity is impaired. These findings show that osteoclasts require their entire integrin repertoire to be regulated by kindlin-3 to orchestrate bone homeostasis.

Introduction

Integrins are α/β heterodimeric cell surface receptors that bind extracellular matrix proteins and cell counter receptors. A hallmark of integrins is their ability to reversibly shift between different affinity states for their ligands. The shift from an inactive to an active conformation is triggered by the direct binding of talin and kindlin to the cytoplasmic domains of β1, β2, and β3 integrins, and is called integrin inside-out signaling (Moser et al., 2009b). Active integrins recruit and assemble large multimolecular complexes at their short cytoplasmic domains controlling several cellular processes such as organization of the cytoskeleton, migration, proliferation, differentiation, and apoptosis (integrin outside-in signaling; Legate et al., 2009).

Kindlins are a family of evolutionary conserved, intracellular FERM (4.1, ezrin, radixin, moesin) domain–containing proteins that are recruited to integrin adhesion sites (Moser et al., 2009b). Mammals have three members, called kindlin-1, -2, and -3. In contrast to the widely expressed kindlin-1 and -2, kindlin-3 expression is restricted to hematopoietic cells (Weinstein et al., 2003; Ussar et al., 2006). The importance of kindlin-3 for integrin activation in vivo was first described in kindlin-3–deficient mice, which suffer from bleeding and leukocyte adhesion defects (Moser et al., 2008, 2009a). Further cellular and molecular analyses of mouse and human blood cells revealed that kindlin-3 is required for activation of αIIbβ3 on platelets and β2 integrins on leukocytes (Moser et al., 2009b). Based on these findings, several groups identified mutations in the human kindlin-3 gene in patients with leukocyte adhesion deficiency (LAD) type III syndrome, which

Correspondence to Markus Moser: moser@biochem.mpg.de

Abbreviations used in this paper: AP, alkaline phosphatase; FAK, focal adhesion kinase; GAPDH, glyceraldehyde 3-phosphate dehydrogenase; LAD, leukocyte adhesion deficiency; M-CSF, macrophage-colony stimulating factor; MMP, matrix metalloproteinase; ON, overnight; OPG, osteoprotegerin; pQCT, peripheral quantitative computer tomography; PTH, parathyroid hormone; RANKL, receptor activator of nuclear factor κB ligand; TRAP, tartrate-resistant acid phosphatase; WASp, Wiskott-Aldrich syndrome protein.

The Rockefeller University Press $30.00
J. Cell Biol. Vol. 192 No. 5 883–897
www.jcb.org/cgi/doi/10.1083/jcb.201007141

is characterized by recurrent bacterial and fungal infections and severe bleeding (Kuijpers et al., 2009; Malinin et al., 2009; Moser et al., 2009a; Svensson et al., 2009). In addition to the severe platelet and leukocyte dysfunction, increased bone mass was observed in several LAD-III patients (Kilic and Etzioni, 2009; McDowall et al., 2010; Sabnis et al., 2010). It was recently proposed that the osteopetrosis is caused by increased osteogenic potential of mesenchymal stem cells (Malinin et al., 2009).

Bone remodeling depends on a tight interplay of osteoblasts that form bone and osteoclasts that resorb bone. Osteoblasts are derived from mesenchymal stem cells and cluster their integrins in adhesion sites termed focal adhesions (FAs). Osteoclasts are large, multinucleated cells that derive from the monocyte lineage and arrange their integrins in adhesion structures called podosomes. Podosomes contain a dotlike core of actin filaments, which is perpendicularly oriented to the plasma membrane and surrounded by a ringlike arrangement of adhesion, adaptor, and signaling molecules such as integrins, paxillin, vinculin, talin, protein kinases, and actin-associated molecules (Linder and Kopp, 2005). Podosomes are found in all cells of the monocytic cell lineage (macrophages, dendritic cells, etc.), smooth muscle cells, endothelial cells, src-transformed fibroblasts, and certain epithelial cells (Linder and Aepfelbacher, 2003). Bone-resorbing osteoclasts arrange their podosomes by interconnecting the actin cytoskeleton into densely packed rings called sealing zones. They delineate the active sites of bone resorption and form a pocket, into which protons and bone-resorbing proteases are secreted (Luxenburg et al., 2007). Sealing zones are attached to the bone matrix via αvβ3 integrin. Although mature osteoclasts express integrins of the β1, β2, and αv families, it is believed that αvβ3 integrins are the major adhesion proteins in osteoclast biology. This observation is largely based on the matrix degradation defects observed in Glanzmann patients or mice carrying null mutations in the β3 integrin gene. The reduced resorptive activity was thought to be caused by loss of αvβ3-mediated signaling that regulates cell polarity and cytoskeletal reorganization (McHugh et al., 2000; Faccio et al., 2003a). It cannot be excluded, however, that β1 and/or β2 integrins also play a role in osteoclast-mediated bone resorption in vivo (Helfrich et al., 1996; Rao et al., 2006).

Increased bone mineralization has been proposed to be the cause for the osteopetrosis in LAD-III patients (Malinin et al., 2009). It remains unclear, however, whether loss of kindlin-3 is indeed responsible for the increased bone mass and whether this bone abnormality is caused by an osteoblast and/or osteoclast dysfunction. In this paper, we find that kindlin-3–deficient mice develop a severe osteopetrotic phenotype caused by osteoclast dysfunctions. We show that kindlin-3–deficient osteoclasts fail to activate all their integrin classes, which in turn leads to their inability to spread and reorganize the actin cytoskeleton, as well as a failure to form podosomes and sealing zones and to degrade bone matrix. Our results indicate that all integrin classes are required for osteoclast-mediated bone resorption.

Results

Kindlin-3–deficient mice develop severe osteopetrosis

Kindlin-3–deficient (kindlin-3$^{-/-}$) mice die a few days after birth because of a severe anemia caused by massive bleeding and erythrocyte defects (Krüger et al., 2008; Moser et al., 2008). To analyze whether kindlin-3 affects bone development, we performed histology and peripheral quantitative computer tomography (pQCT) on long bones from kindlin-3$^{-/-}$ mice. At postnatal day 4 (P4), kindlin-3$^{-/-}$ bones showed a significant increase in trabecular bone accompanied by a marked decrease in bone marrow (Fig. 1 A). Van Kossa staining showed increased calcified bone (Fig. 1 B). pQCT analysis confirmed a significant increase in bone mineral density (BMD; Fig. 1 C). Bone surface as determined by static histomorphometry was markedly increased in the absence of kindlin-3 (Fig. 1 D).

To define the onset of the osteopetrosis, we compared the histology of control and mutant long bones from different developmental stages. At embryonic day 14 (E14), long bones from kindlin-3$^{-/-}$ embryos showed normal primary ossification centers surrounded by a normal coat of membranous bone (Fig. S1 A). At E16, kindlin-3$^{-/-}$ bones displayed increased ossification, and at birth, the bone mass further increased at the expense of the bone marrow cavity (Fig. S1 A). Alkaline phosphatase (AP) staining of osteoblasts and tartrate-resistant acid phosphatase (TRAP)-positive osteoclasts did not significantly differ between control and mutant bones at E14, E16, and P1 (Fig. S1, A and B).

Loss of kindlin-3 leads to severe osteoclast dysfunction

It has been proposed that a dysfunction of osteoblasts is responsible for increased bone density in LAD-III patients (Malinin et al., 2009). To test whether this is also the case in kindlin-3$^{-/-}$ mice, we performed histomorphometric analysis, which showed normal osteoblast numbers per unit of bone surface in kindlin-3$^{-/-}$ bones (Fig. S2 A). Calvaria-derived osteoblasts isolated from wild-type and kindlin-3$^{-/-}$ pups revealed comparable levels of gene expression for osteoblastic markers such as AP, osteocalcin, and collagen I as well as normal AP activity (Fig. S2, B, D, and E). Furthermore, the generation of mineralized bone nodules in vitro was similar in osteoblasts from both genotypes. (Fig. S2, F–H). Finally, and in line with the normal biological activity of kindlin-3$^{-/-}$ osteoblasts, wild-type osteoblasts expressed kindlin-2 but neither kindlin-3 nor kindlin-1 (Fig. S2 C).

To determine whether osteoclasts are defective, we performed TRAP staining and histomorphometric measurements of P4 kindlin-3$^{-/-}$ bones, which revealed that the number of TRAP-positive osteoclasts per bone surface was significantly increased by more than threefold (Fig. 1, E and F). Despite the elevated number of osteoclasts, the surface covered by osteoclasts was significantly decreased in kindlin-3$^{-/-}$ bones (Fig. 1 G). Consistent with the failure to erode bone, Ca^{2+} levels in the serum of kindlin-3$^{-/-}$ mice were significantly decreased (Fig. 1 H), and parathyroid hormone (PTH) levels were increased (Fig. 1 I). Indeed, cultured osteoclasts differentiated from wild-type blood

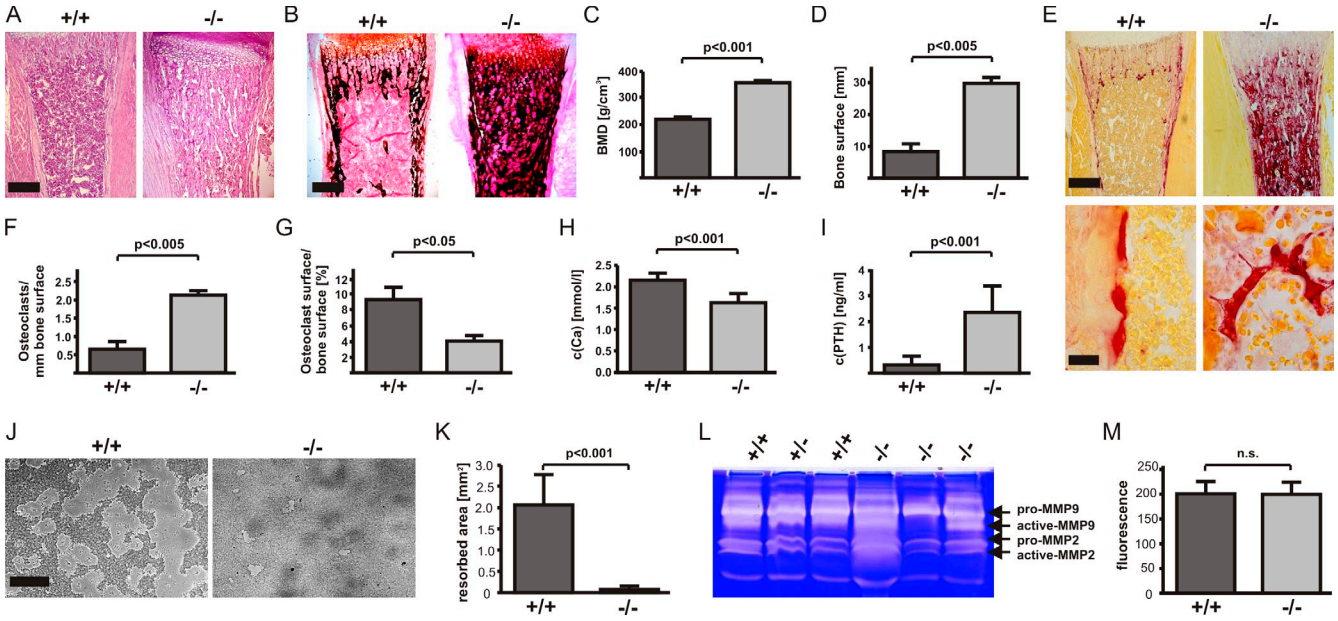

Figure 1. **Kindlin-3$^{-/-}$ mice develop severe osteopetrosis.** (A and B) Histology of tibiae of P4 wild-type and kindlin-3$^{-/-}$ mice stained with hematoxylin and eosin (A) and van Kossa (B). (C and D) Quantitative peripheral computer tomography measurements determining bone mineral density (C) and histomorphometric analysis to determine bone surface from bones of P4 wild-type and kindlin-3$^{-/-}$ mice (D); $n = 3$. (E) Histology of tibiae of P4 wild-type and kindlin-3$^{-/-}$ mice stained for TRAP activity. (F and G) Histomorphometric analyses determining the number of osteoclasts (F) and surface covered by osteoclasts (G) of wild-type and kindlin-3$^{-/-}$ mice; $n = 3$. (H) Ca^{2+} levels in serum of P4 wild-type and kindlin-3$^{-/-}$ mice; $n = 8$. (I) PTH levels in plasma of P3 wild-type and kindlin-3$^{-/-}$ mice; $n = 10$. (J and K) Resorption pits (J) and their quantification (K) of wild-type and kindlin-3$^{-/-}$ osteoclasts cultured on calcium apatite coated slides; $n = 7$. (L) Zymography of cell culture supernatants from primary wild-type and kindlin-3$^{-/-}$ osteoclasts. (M) Cathepsin K activity from lysates of primary wild-type and kindlin-3$^{-/-}$ osteoclasts; $n = 11$. Data are presented as mean ± SD (error bars). P-values indicate significant differences from wild-type (Student's *t* test). n.s., not significant. Bars: (A and B) 250 µm; (E, top) 250 µm; (E, bottom) 25 µm; (J) 100 µm.

precursors expressed high levels of kindlin-3 but neither kindlin-1 nor -2 (Fig. 2 B and Fig. S2 C).

These data suggest that kindlin-3$^{-/-}$ osteoclasts are functionally impaired. To address this finding, we tested the resorptive activity of kindlin-3$^{-/-}$ osteoclasts by seeding them on an artificial calcified matrix (osteologic slides) as well as dentin discs. Although wild-type osteoclasts resorbed large areas of mineralized matrix, kindlin3$^{-/-}$ osteoclasts were incapable of doing so (Fig. 1 J and not depicted). Morphometric image analysis of the resorbed areas revealed that resorption by kindlin-3$^{-/-}$ osteoclasts was >20-fold lower than wild-type cells (Fig. 1 K). The profound resorption defects were not accompanied by diminished secretion of proteolytic enzymes, as secretion of matrix metalloproteinase 2 (MMP2) and -9 and cathepsin K activities were indistinguishable between control and kindlin-3$^{-/-}$ osteoclasts (Fig. 1, L and M).

Altogether, these findings indicate that osteopetrosis in kindlin-3$^{-/-}$ mice is caused by a dysfunction of osteoclasts rather than osteoblasts.

Kindlin-3 is not required for osteoclast differentiation

Osteoclasts originate from monocytic precursors in response to the actions of macrophage-colony stimulating factor (M-CSF) and receptor activator of nuclear factor κB ligand (RANKL; Teitelbaum and Ross, 2003). Although the serum levels of M-CSF were similar (unpublished data), circulating levels of RANKL were increased eightfold in kindlin-3$^{-/-}$ mice (Fig. 2 A). Serum concentrations of osteoprotegerin (OPG), an inhibitor of RANKL, were similar between wild-type and kindlin-3$^{-/-}$ mice. Treatment of kindlin-3$^{-/-}$ osteoclasts with RANKL in vitro induced a strong and sustained p38 and JNK phosphorylation that was comparable to wild-type osteoclasts (Fig. S3). The high levels of RANKL in the serum and the normal response to RANKL by kindlin-3$^{-/-}$ osteoclasts provides a plausible explanation for the increased osteoclastogenesis in kindlin-3$^{-/-}$ bones.

M-CSF and RANKL treatment induced the expression of osteoclastogenic markers such as cathepsin K, MMP9, and calcitonin receptor in wild-type and kindlin-3$^{-/-}$ fetal liver cells (Fig. 2 B). Even though induction of marker gene expression was slightly delayed in kindlin-3$^{-/-}$ cells, they nevertheless reached wild-type levels 6 d after cytokine treatment (Fig. 2 B). It should be noted that the expression of kindlin-3 remained stable throughout the differentiation period, and that kindlin-1 and -2 were expressed in neither wild-type nor kindlin-3$^{-/-}$ cells upon cytokine treatment (Fig. 2 C).

Finally, we determined the number of nuclei in the osteoclasts as a marker for pre-osteoclast fusion and differentiation. Notably, in vitro generated kindlin-3$^{-/-}$ osteoclasts showed a lower tendency to form larger (>20 nuclei) polykaryons (Fig. 2 D), presumably because of decreased adhesion and cell spreading; however, a significant shift toward more multinucleated osteoclasts was detected in bone sections from kindlin-3$^{-/-}$ mice (Fig. 2 E). This discrepancy can be explained by the increased number of osteoclast precursors triggered by the elevated RANKL levels in kindlin-3$^{-/-}$ mice.

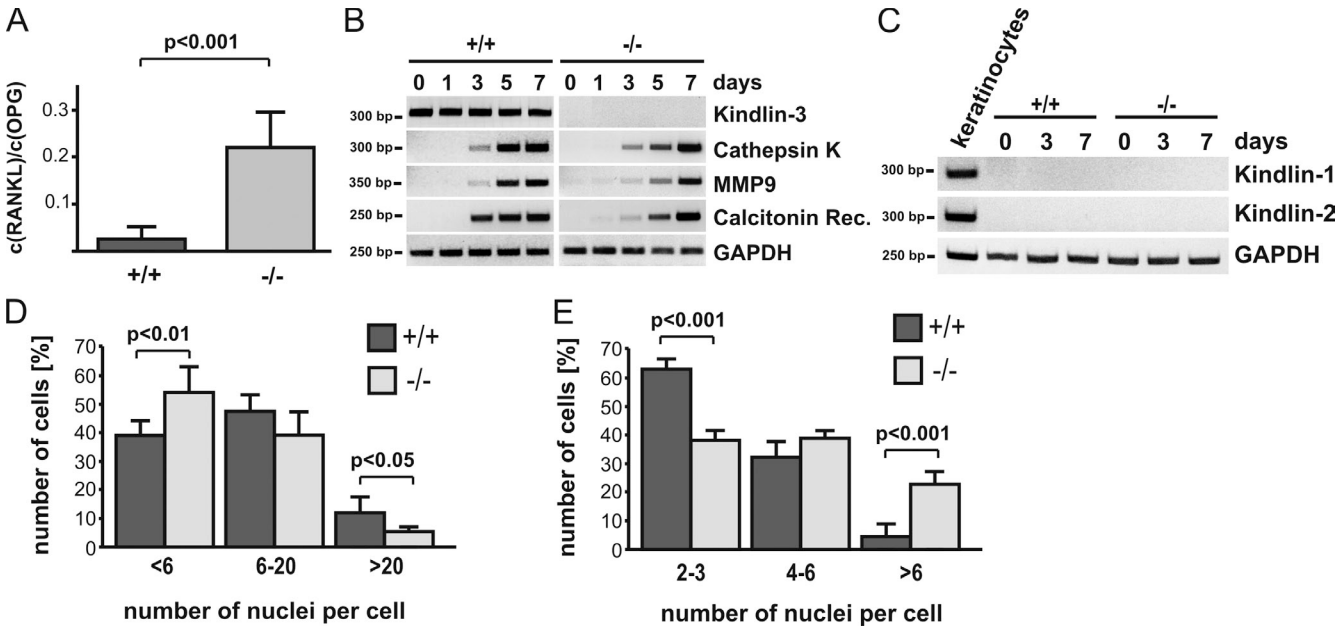

Figure 2. **Differentiation of kindlin-3$^{-/-}$ osteoclasts.** (A) RANKL/OPG ratio in plasma of P3 wild-type and kindlin-3$^{-/-}$ mice; n = 11. (B) RT-PCR of osteoclastogenic markers upon M-CSF and RANKL treatment of wild-type and kindlin-3$^{-/-}$ fetal liver cells. (C) RT-PCR of kindlin-1 and -2 expression during in vitro osteoclast differentiation. RNA from keratinocytes served as positive control. (D) Number of nuclei per osteoclast 5 d after induction of differentiation; 1,004 cells of each genotype obtained from five independent experiments were analyzed. (E) Osteoclast nuclear numbers determined from histological sections of P4 tibiae. 63 and 252 osteoclasts from wild-type and kindlin-3$^{-/-}$ bone sections were analyzed, respectively. Data are presented as mean ± SD (error bars). P-values indicate significant differences from wild-type (Student's t test).

Altogether, these data suggest that although osteoclast differentiation is slightly delayed in the absence of kindlin-3 in vitro, it occurs efficiently in kindlin-3$^{-/-}$ mice.

Kindlin-3 promotes osteoclast adhesion by regulating integrin activation

Kindlin-3 is required for the activation of integrins and integrin-mediated adhesion (Moser et al., 2008, 2009a). To evaluate osteoclast adhesion, we seeded wild-type and kindlin-3$^{-/-}$ osteoclasts on osteopontin, a natural ligand for osteoclasts. Although wild-type osteoclasts adhered readily to osteopontin, kindlin-3$^{-/-}$ osteoclasts showed significantly reduced adhesion (Fig. 3 A). Interestingly, kindlin-3$^{-/-}$ osteoclasts adhered to both glass and cell culture plastic, particularly when cultured over several days. Because the transmembrane proteoglycan CD44 has also been shown to support osteoclast adhesion to osteopontin, fibronectin, collagen, and laminin (Goodison et al., 1999; Ponta et al., 2003), we hypothesized that CD44 might mediate the remaining osteoclast adhesion in the absence of kindlin-3. To test this hypothesis, we incubated pre-osteoclasts with a blocking anti-CD44 antibody and observed that the adhesion of kindlin-3$^{-/-}$ cells to fibronectin was further reduced, which indeed indicates that CD44 contributes to osteoclast adhesion (Fig. S4, A and B).

To determine integrin expression, we measured their levels on macrophages, as the large size and strong adhesive properties of mature osteoclasts prevented their analysis by flow cytometry. Indeed, kindlin-3$^{-/-}$ macrophages express ∼76% and 63% of β1 and β3 integrins, respectively, when compared with wild-type macrophages. The expression of αvβ5, which decreases during osteoclast maturation, and α4β1, α5β1, and αLβ2 were similar in wild-type and kindlin-3$^{-/-}$ cells; however, αMβ2 was reduced to ∼80% in kindlin-3$^{-/-}$ cells. (Fig. 3 B and Fig. S4 C). Next, we addressed the affinity states of integrins by determining the binding of the 9EG7 antibody, which recognizes activated mouse β1 integrins, and the binding of a fluorescently labeled FN fragment (FNIII7-10), which is bound by active αv (αvβ3 and αvβ5) and α5β1 integrins. Resting kindlin-3$^{-/-}$ macrophages failed to bind 9EG7 and showed considerably reduced FNIII7-10 binding, whereas $MnCl_2$ treatment, which can bypass inside-out–mediated integrin activation, markedly increased 9EG7 and FNIII7-10 binding (Fig. 3, C and D). Furthermore, adhesion to ICAM-1, a ligand for β2 integrins, was strongly diminished in kindlin-3$^{-/-}$ macrophages compared with control cells (Fig. 3 E). Manganese treatment only partially rescued the adhesion defect of kindlin-3$^{-/-}$ cells, which suggests that kindlin-3 also operates in integrin outside-in signaling.

Collectively, these data indicate that loss of kindlin-3 results in a severe adhesion defect caused by impaired activation and outside-in signaling of β1, β2, and αv integrins.

Osteoclasts require kindlin-3 for integrin and growth factor signaling

Biochemical signaling events triggered by integrins and growth factor receptors control osteoclast adhesion, spreading, fusion, and differentiation (Ross and Teitelbaum, 2005). Wild-type osteoclasts generated from fetal liver cells differentiated into well-spread, multinucleated osteoclasts within 4–6 d of culture (Fig. 4 A). In contrast, kindlin-3$^{-/-}$ fetal liver cells, which also

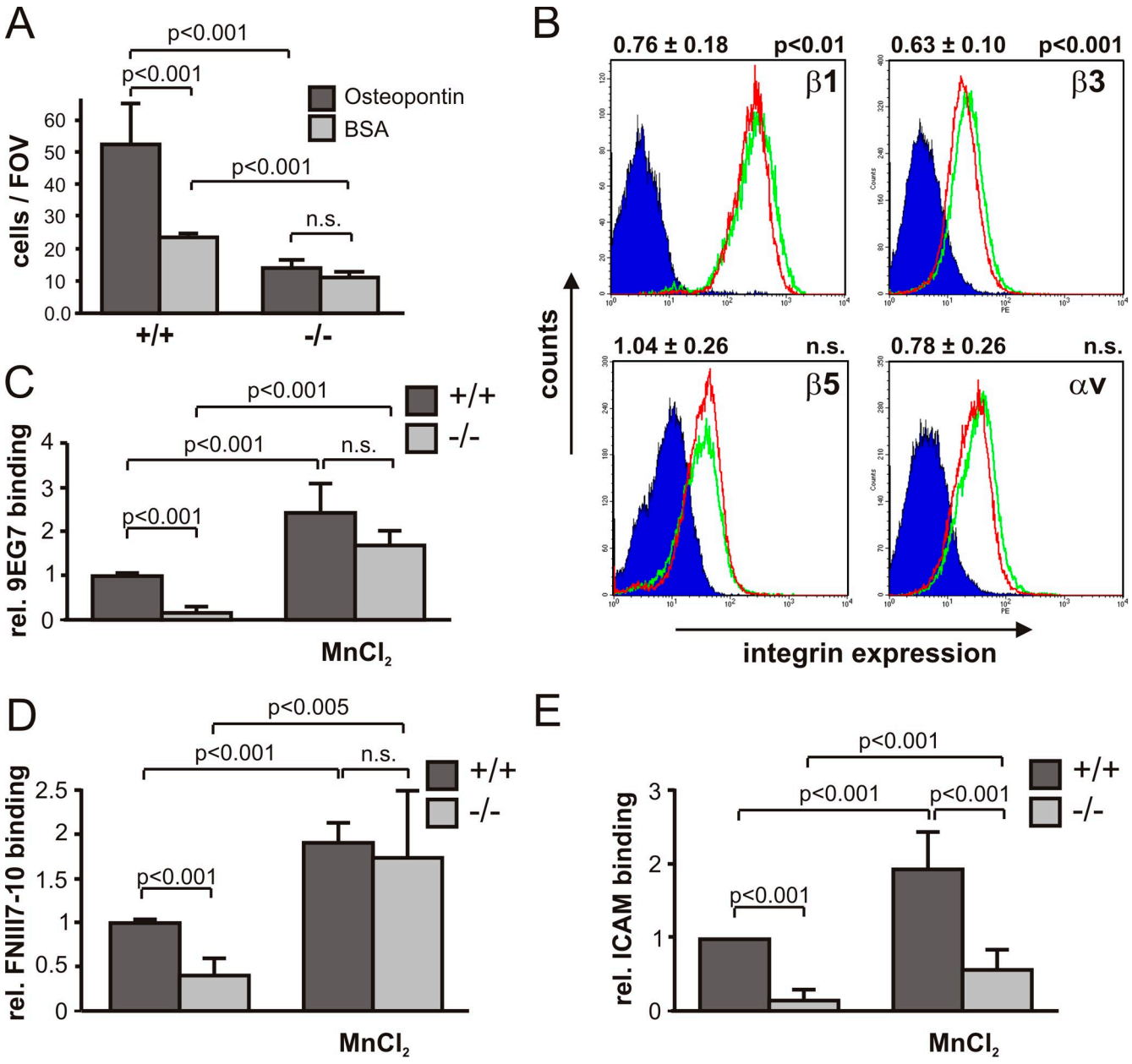

Figure 3. **Integrin defects in kindlin-3$^{-/-}$ osteoclasts.** (A) Adhesion of primary wild-type and kindlin-3$^{-/-}$ osteoclasts to osteopontin. Number of adherent cells per field of view (FOV) is shown. (B) Surface expression of β1, β3, β5, and αV integrins on wild-type (green) and kindlin-3$^{-/-}$ (red) macrophages. Isotype control staining is shown in dark blue. Numbers above graphs indicate integrin expression on kindlin-3$^{-/-}$ cells (mean ± SD) relative to wild-type cells (n = 6). (C) 9EG7 binding on wild-type and kindlin-3$^{-/-}$ macrophages in the presence or absence of 2 mM $MnCl_2$. (D) Binding of Alexa Fluor 647–labeled FNIII7-10 by wild-type and kindlin-3$^{-/-}$ macrophages in the presence or absence of 3 mM $MnCl_2$. Data show mean ± SD of four independent experiments and were subtracted by background binding of the isotype and EDTA control, respectively. (E) Wild-type and kindlin-3$^{-/-}$ macrophages plated on ICAM-1 in the presence or absence of 1 mM $MnCl_2$. P-values indicate significant differences from wild-type (Student's t test).

produced multinucleated TRAP-positive cells, failed to spread (Fig. 4 A). Phalloidin staining showed an actin belt beneath the plasma membrane of control osteoclasts, whereas kindlin-3$^{-/-}$ osteoclasts displayed randomly distributed actin patches in their cytoplasm (Fig. 4 B). Mn^{2+}-mediated activation of integrins was unable to improve the spreading defect, suggesting that kindlin-3 is also required for integrin outside-in signaling, which is central in organizing the osteoclast cytoskeleton (unpublished data). Retroviral expression of EGFP–kindlin-3 into kindlin-3$^{-/-}$ fetal liver cells rescued the formation of well-spread osteoclasts. Notably, expression of integrin-binding mutant EGFP–kindlin-3 (EGFP–kindlin-3–QA; Moser et al., 2008) did not rescue osteoclast spreading, whereas fusion significantly improved compared with cells infected with a control virus (Fig. S5, A and B).

Next, we analyzed whether integrin-mediated adhesion signaling can still occur in the absence of kindlin-3. Adhesion on vitronectin triggered phosphorylation of c-Src and focal adhesion kinase (FAK) in wild-type pre-osteoclasts, but induced only a weak phosphorylation in kindlin-3$^{-/-}$ pre-osteoclasts

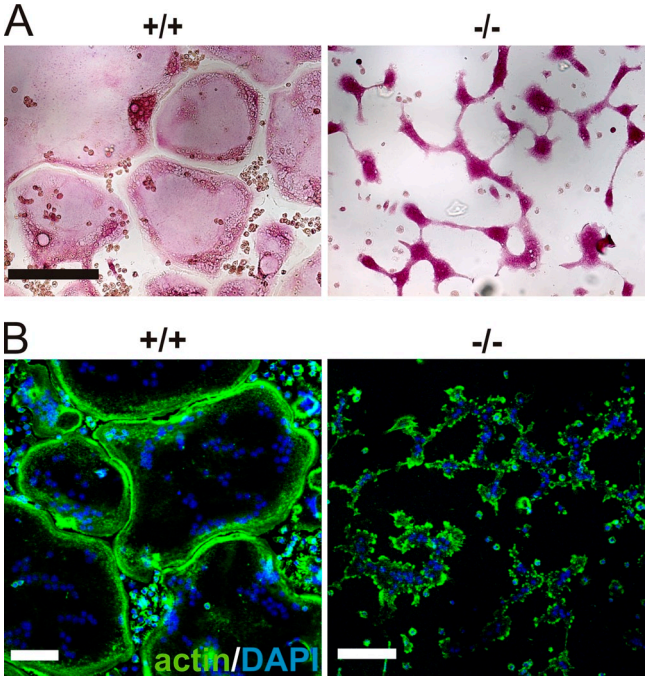

Figure 4. **Defective spreading of kindlin-3$^{-/-}$ osteoclasts.** (A) Wild-type and kindlin-3$^{-/-}$ osteoclasts grown on glass coverslips and stained for TRAP. (B) F-actin (stained with phalloidin, green) and nuclei (DAPI, blue) in wild-type and kindlin-3$^{-/-}$ osteoclasts. Bars, 100 µm.

(Fig. 5 A), further corroborating the finding that integrin-mediated signaling is severely compromised in the absence of kindlin-3. This weak activation is either triggered by integrin-independent signaling processes or by some residual integrin activity that exists even in the absence of kindlin-3.

A previous study demonstrated that loss of αvβ3 integrin function in osteoclasts can be compensated by high concentrations of M-CSF (Faccio et al., 2003b). To test whether kindlin-3 loss can also be overcome by high levels of cytokines, we treated wild-type and mutant fetal liver cells with RANKL and different concentrations of M-CSF. Wild-type fetal liver cells differentiated within 4 d into large, multinucleated osteoclasts when cultured at low M-CSF levels (20 ng/ml), whereas kindlin-3$^{-/-}$ fetal liver cells rarely fused into polykaryons. High levels of M-CSF (100 ng/ml) rescued polykaryon formation but not the spreading defect of kindlin-3$^{-/-}$ cells (Fig. 5 B). Moreover, although low levels of M-CSF failed to induce normal phosphorylation of Erk, Akt, and Syk in kindlin-3$^{-/-}$ osteoclasts, high levels were able to induce normal phosphorylation of these signaling proteins (Fig. 5 C), which suggests normal differentiation of kindlin-3$^{-/-}$ osteoclasts in the presence of high M-CSF levels.

Altogether, these findings show that kindlin-3 recruitment to integrins is required for their activation, actin reorganization, and cell spreading, as well as amplification of growth factor signaling in osteoclasts.

Kindlin-3 is required for the formation and arrangement of podosomes

Osteoclast adhesion is mediated by the formation of specialized adhesion structures called podosomes when they are cultured on glass or bone matrix. Wild-type pre-osteoclasts were able to form typical podosomes consisting of a central actin core surrounded by a ring of adhesion molecules including αv(β3) and β1 integrins, vinculin, paxillin, and talin (Fig. 6, A, C, and D; and not depicted). Kindlin-3$^{-/-}$ cells formed small, actin core–like structures surrounded by a diffuse actin cloud. Vinculin, talin, and paxillin colocalized with the actin cloud, whereas αv and β1 integrins were diffusely distributed throughout the plasma membrane (Fig. 6, A, C, and D; and not depicted). Fluorescence intensity profiling through actin-core units revealed that actin cores alternate with vinculin rings in wild-type podosomes, whereas this alternating pattern of actin and vinculin staining was lost in kindlin-3$^{-/-}$ cells (Fig. 6 B). Approximately half (59.9% ± 11.1%) of the actin dots from kindlin-3$^{-/-}$ cells were depleted of vinculin and considered to be podosome structures even though a discrete vinculin ring was rarely observed. Re-expression of GFP–kindlin-3 into kindlin-3$^{-/-}$ pre-osteoclasts restored the size of the F-actin dots and the ringlike distribution of vinculin around the F-actin cores (Fig. S5 C). On the contrary, the integrin-binding mutant EGFP–kindlin-3–QA did not rescue podosome formation in kindlin-3$^{-/-}$ pre-osteoclasts and showed a diffuse distribution throughout the cell membrane when expressed in control pre-osteoclasts (Fig. S5 C). The percentage of cells that form normal podosomes was similar in EGFP–kindlin-3–expressing control and kindlin-3$^{-/-}$ cells, whereas re-expression of the EGFP–kindlin-3–QA resulted in significantly fewer podosome-forming cells (Fig. S5 D). Re-expression of the integrin-binding mutant kindlin-3 did just partially improve the diffuse vinculin and F-actin localization in kindlin-3$^{-/-}$ cells (Fig. S5 C). In line with the normal podosome formation in EGFP–kindlin-3–expressing kindlin-3$^{-/-}$ cells, αv integrins colocalized with vinculin to podosome rings, whereas αv integrins were diffusively distributed in the membrane of kindlin-3$^{-/-}$ cells expressing an EGFP–kindlin-3–QA construct (Fig. S5 E). Finally, the resorptive activity of kindlin-3$^{-/-}$ osteoclasts expressing an EGFP–kindlin-3–QA was five times less compared with kindlin-3–deficient osteoclasts expressing wild-type EGFP–kindlin-3 (Fig. S5 F).

High-resolution scanning electron microscopy confirmed that kindlin-3$^{-/-}$ osteoclasts were able to form small actin patches, which were surrounded by a loose network of radial actin fibers (Fig. 7 A). In sharp contrast, control osteoclasts formed large actin cores within podosome clusters, which were extensively interconnected by thick actin bundles (Fig. 7 A). Despite their smaller size, the actin cores of kindlin-3$^{-/-}$ cells colocalized with cortactin, Arp2/3, and Wiskott-Aldrich syndrome protein (WASp), which are known core components of podosomes (Linder and Aepfelbacher, 2003), indicating that podosomal actin core formation occurs in the absence of kindlin-3 and activated integrins (Fig. 7, B–D).

Mature osteoclasts arrange their podosomes into different higher ordered structures. On glass, they form a ring at the periphery of the cell called the podosomal belt (Fig. 8 A); whereas on mineralized matrices, they form several smaller ringlike adhesion structures called sealing zones (Fig. 8 B; Jurdic et al., 2006). Kindlin-3$^{-/-}$ osteoclasts were not able to form podosomal rings on glass surfaces or on sealing zones

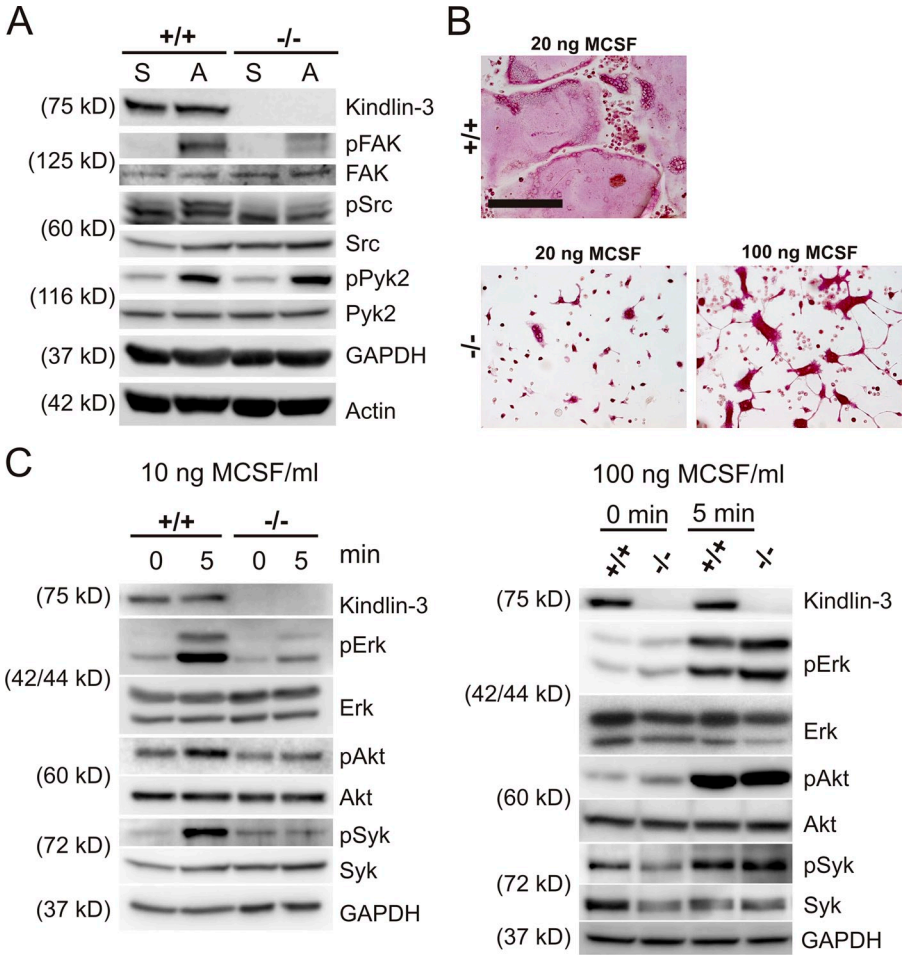

Figure 5. **Impaired adhesion and M-CSF signaling in kindlin-3$^{-/-}$ pre-osteoclasts.** (A) Wild-type and kindlin-3$^{-/-}$ pre-osteoclasts either maintained in suspension (S) or replated on vitronectin (A). Western blotting for kindlin-3, p-FAK, FAK, p-src, Src, p-Pyk2, and Pyk2. GAPDH and actin served as loading controls. (B) TRAP staining of wild-type and kindlin-3$^{-/-}$ osteoclasts treated with 40 ng/ml RANKL together with either 20 ng/ml or 100 ng/ml M-CSF. Bar, 250 µm. (C) Starved wild-type and kindlin-3$^{-/-}$ osteoclasts treated with either 10 ng/ml or 100 ng/ml M-CSF. Western blotting for activated Erk and Akt. Activated Syk was determined by immunoprecipitation followed by immunoblotting with anti-phosphotyrosine (4G10) antibody.

on bone matrices. F-actin and vinculin often colocalized in patches and were usually localized to the cell periphery (Fig. 8, A and B). The formation of podosomal belts and sealing zones requires an intact microtubule network (Destaing et al., 2003, 2005). We therefore analyzed microtubule organization and acetylation by immunofluorescence microscopy and Western blot analysis. Both the total and acetylated microtubule pools were similar between kindlin-3$^{-/-}$ and wild-type osteoclasts (Fig. 8, C and D). Furthermore, phosphorylation and the total amount of Pyk2, which is required for microtubule stability and acetylation in osteoclasts (Gil-Henn et al., 2007), were not altered in kindlin-3$^{-/-}$ cells (Fig. 5 A), an observation that was also made in β3 integrin–deficient osteoclasts (Faccio et al., 2003a).

These data indicate that kindlin-3 is not required for initial actin core formation. However, actin core maturation and interconnection, podosome formation, and their subsequent assembly into belts and sealing zones depend on kindlin-3.

β1, β2, and αv integrin classes are required for normal osteoclast function

αvβ3 integrin is considered the major functional integrin on osteoclasts. In contrast to the severe osteopetrotic phenotype of kindlin-3–deficient mice, however, loss of αvβ3 leads to a mild and protracted osteopetrosis in mice and humans. This discrepancy led us to hypothesize that additional integrins contribute to the kindlin-3$^{-/-}$ osteoclast defect. To test this, we established osteoclast cultures from mice lacking the β1, β2, or αv integrin genes, respectively, and from mice lacking a combination of two or all three integrin genes. In addition, we generated osteoclasts from β3 integrin–deficient mice to test whether other αv integrins in addition to αvβ3 play a significant role in osteoclast biology. Bone marrow cells with a single or αv/β1 or β1/β2 double integrin-null mutation differentiated into multinucleated, spread, and TRAP-positive osteoclasts. Osteoclasts lacking both αv and β2 integrins formed polykaryons but were less efficient in spreading and localizing their nuclei to the cell periphery (Fig. 9 A). Bone marrow cells lacking β1/β2/αv integrins were only able to form a few mono- and binucleated cells with TRAP activity, which suggests that loss of all integrin classes severely impairs osteoclastogenesis in vitro (Fig. 9 A). Notably, although these cells did not spread, they weakly adhered on glass.

Individual podosomes, podosome clusters, and podosome belts of β1, β2, and β1/β2 double integrin-null cells were indistinguishable from wild-type cells. αv- and β3-deficient cells showed smaller podosome clusters with irregular distributed podosome units (Fig. 9 B). Deletion of αv together with β1 or β2 integrins abolished cluster formation completely, and typical podosomes with a discrete vinculin ring were rarely

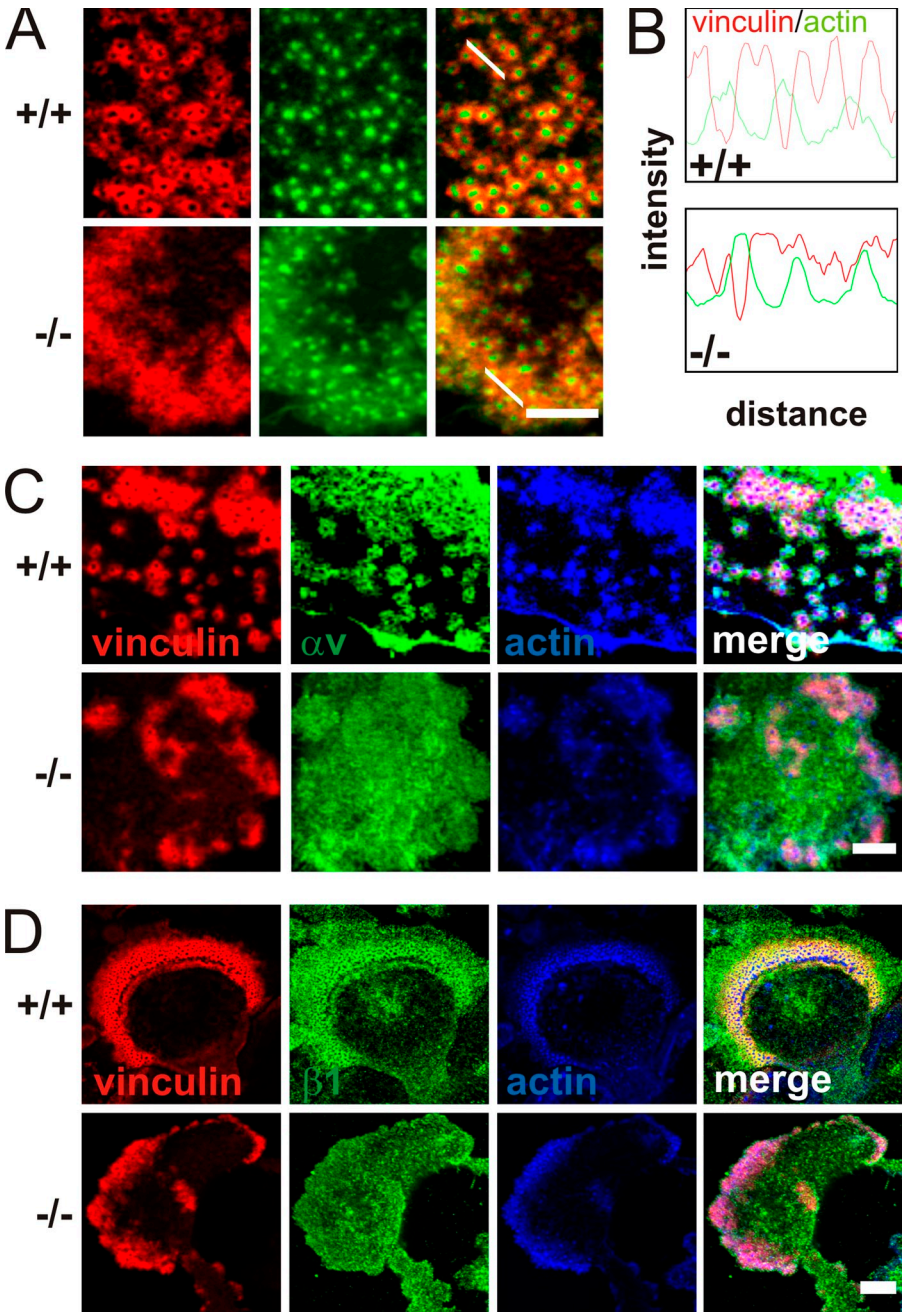

Figure 6. **Impaired podosome formation in kindlin-3$^{-/-}$ osteoclasts.** (A) Vinculin (red) and F-actin staining (phalloidin, green) of pre-osteoclasts plated on glass coverslips and observed by confocal microscopy. (B) Fluorescence intensity profile through three actin-core units (indicated by the white lines in A) of wild-type and kindlin-3$^{-/-}$ pre-osteoclasts. (C and D) vinculin (red) and F-actin staining (phalloidin, blue) together with αv integrin (green; C) or β1 integrin (green; D). Bars (A and C) 5 µm; (D) 10 µm.

observed (Fig. 9 B). Similar to loss of kindlin-3, cells lacking β1/β2/αv integrins formed small actin dots lacking an adhesion ring (Figs. 9 B and 6 A). In agreement with these observations, we found that the diameter of the actin core was significantly smaller (~650 nm) in podosomes from kindlin-3$^{-/-}$, β1/β2/αv triple-null, and αv/β1 and αv/β2 double-null pre-osteoclasts when compared with wild-type cells (~800 nm) or cells with a single integrin or a double β1/β2 integrin gene ablation (Fig. 9 C). Podosome belts of αv-deficient cells often failed to surround the entire cell and were significantly thinner than belts from β3-deficient cells, which showed a belt size that was intermediate between control and αv-deficient osteoclasts (Fig. 9, D and E). αv/β1 as well as αv/β2 integrin–deficient osteoclasts showed even thinner actin belts, which contained fewer and irregularly localized actin dots (Fig. 9, D and E).

Finally, we differentiated bone marrow–derived cells on a calcified matrix and evaluated their sealing zones and their capability to resorb matrix. The absence of a single integrin or the simultaneous loss of β1 and β2 still allowed sealing zone formation (Fig. 10 A), whereas the absence of αv together with either β1 or β2 integrins abolished the formation of a distinct ring (Fig. 10 A). The resorptive activity of αv/β1- and αv/β2-deficient osteoclasts was reduced to 30% of the wild-type level. Despite the presence of sealing zones in single integrin-null osteoclasts, their resorptive activity was diminished by 50%, indicating that each individual integrin family member contributes to functional sealing zone formation and bone degradation (Fig. 10 B).

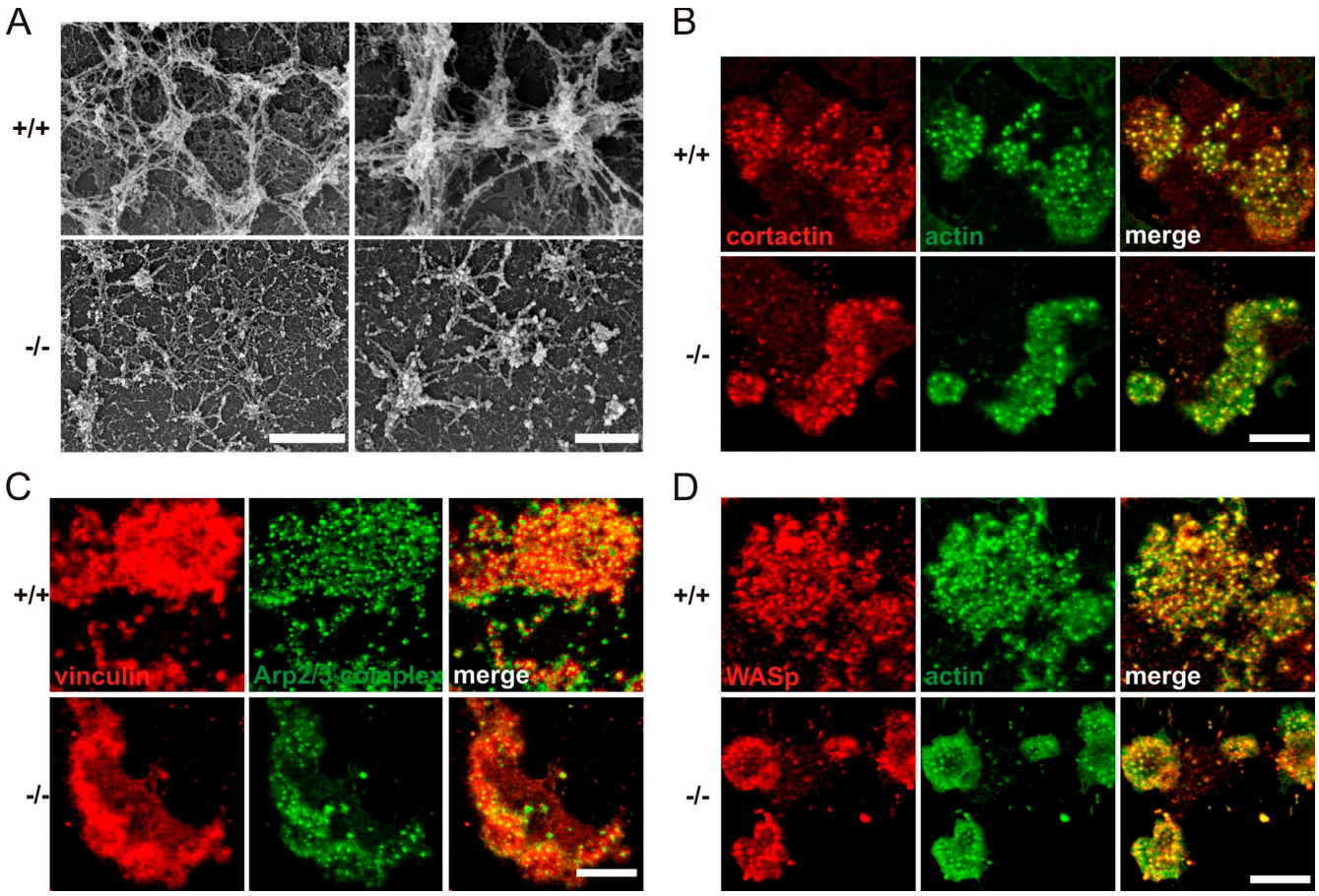

Figure 7. **Podosomal actin core formation is not abolished in kindlin-3$^{-/-}$ cells.** (A) Scanning electron microscopy of basal membrane preparations of wild-type and kindlin-3$^{-/-}$ osteoclasts. (B–D) Colocalization of cortactin (red) and F-actin (phalloidin, green; B), F-actin (red) and Arp2/3 (green; C), and WASp (red) and F-actin (green; D) in podosome clusters of wild-type and kindlin-3$^{-/-}$ pre-osteoclasts analyzed by confocal microscopy. Bars: (A, left) 1 µm; (A, right) 500 nm; (B–D) 10 µm.

Discussion

Several LAD-III patients have displayed increased bone mineral density (Kilic and Etzioni, 2009; Malinin et al., 2009; McDowall et al., 2010; Sabnis et al., 2010), which points to the possibility that kindlin-3 plays a role in bone homeostasis. In search for an explanation of this observation, Malinin et al. (2009) reported that mesenchymal stem cells isolated from LAD-III patients produced significantly higher amounts of cartilage and bone in transplantation experiments, and concluded that the increased bone mass was caused by increased matrix deposition by hyperactive osteoblasts. Although kindlin-3 is highly and exclusively expressed in hematopoietic cells, osteoblasts express kindlin-2 but lack kindlin-3 expression, which suggests that the increased bone mass in LAD-III patients either developed independently of kindlin-3 or was caused by a dysfunction of a cell type other than osteoblasts. In this paper, we tested this hypothesis by analyzing bone formation in mice lacking kindlin-3.

Kindlin-3$^{-/-}$ mice develop a severe osteopetrosis that is already apparent at birth. When we first analyzed the osteoblasts of kindlin-3–deficient mice in vivo and in vitro, we found that they appeared normal in terms of their numbers, morphological appearance, localization to the bone, expression of marker genes, and matrix production. The only abnormality we could detect was a significantly elevated RANKL/OPG ratio in the serum of kindlin-3$^{-/-}$ mice. RANKL secretion by osteoblasts is triggered in response to PTH, which is released by the parathyroid gland when serum Ca^{2+} levels decrease because of diminished bone resorption (Grant et al., 1990; Suda et al., 1999). An immediate consequence of high RANKL levels is enhanced differentiation of osteoclasts, which derive from the monocytic lineage and express high levels of kindlin-3. Indeed, we found reduced levels of Ca^{2+} and markedly increased levels of PTH in the blood of kindlin-3$^{-/-}$ mice. Consistent with the high circulating RANKL levels, we found a dramatic increase in the number of multinucleated osteoclasts in bones of kindlin-3$^{-/-}$ mice. These osteoclasts, however, completely failed to degrade bone matrix in vitro. In search for a mechanistic explanation for the dysfunction of kindlin-3$^{-/-}$ osteoclasts, we identified several cellular defects that could be ascribed to kindlin-3's principal task to activate several classes of integrins and subsequently mediate their outside-in signaling properties.

Our findings show that differentiation of kindlin-3$^{-/-}$ osteoclasts is slightly delayed and that fusion into multinucleated polykaryons is less efficient under in vitro conditions. However, the number of large polykaryons is significantly higher in kindlin-3$^{-/-}$ bones. This is most likely caused by increased RANKL-induced osteoclastogenesis that compensates

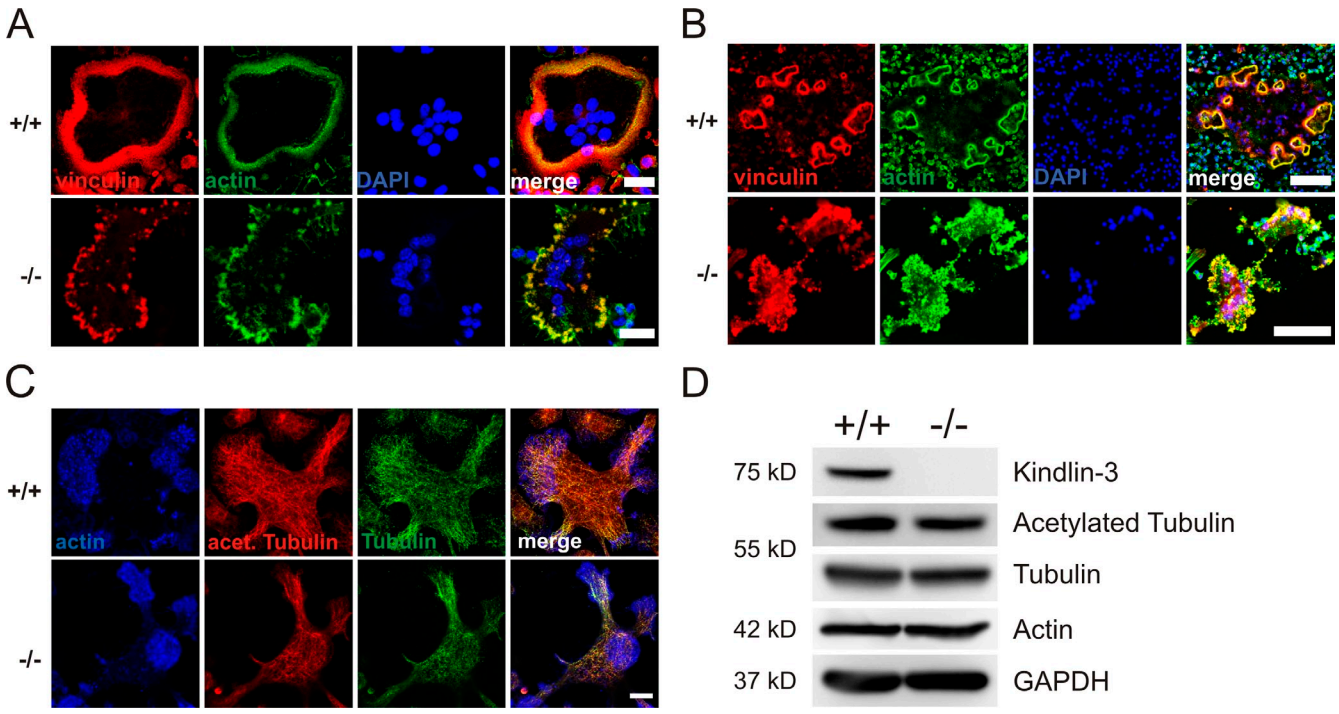

Figure 8. **Abnormal F-actin distribution but normal microtubule organization and acetylation in kindlin-3$^{-/-}$ osteoclasts.** (A) Vinculin (red) and F-actin staining (phalloidin, green) of wild-type and kindlin-3$^{-/-}$ osteoclasts plated on glass coverslips. (B) Vinculin (red) and F-actin staining (phalloidin, green) of wild-type and kindlin-3$^{-/-}$ osteoclasts plated on mineral surface of osteologic slides. DAPI (blue) shows nuclei (A and B). (C) Wild-type and kindlin-3$^{-/-}$ osteoclasts were labeled with phalloidin (blue), anti-acetylated tubulin (green), and anti-tubulin antibodies. (D) Cell lysates from wild-type and kindlin-3$^{-/-}$ osteoclasts were immunoblotted with antibodies against kindlin-3, acetylated tubulin, and tubulin. Antibodies against actin and GAPDH were used as loading controls. Bars: (A) 25 µm; (B) 100 µm; (C) 10 µm.

the fusion defects in vivo. Although TRAP-positive, multinucleated kindlin-3$^{-/-}$ osteoclasts are present at very high numbers in kindlin-3$^{-/-}$ mice, their shape and ability to adhere to bone surfaces is severely impaired. Similarly, adhesion to and binding of several extracellular matrix proteins and to ICAM-1 is also almost completely abrogated. We have previously shown that kindlin-3 interaction with β1 and β3 tails is required to activate platelet integrins and that binding to β2 tails is required to activate leukocyte integrins (Moser et al., 2008, 2009a). Our findings here demonstrate that this essential function of kindlin-3 is also conserved in osteoclasts. Osteoclasts require kindlin-3 to mediate β1 and αv integrin binding to fibronectin and osteopontin and β2 integrin binding to ICAM-1. This suggests that αvβ3 integrins, considered the most important integrin class

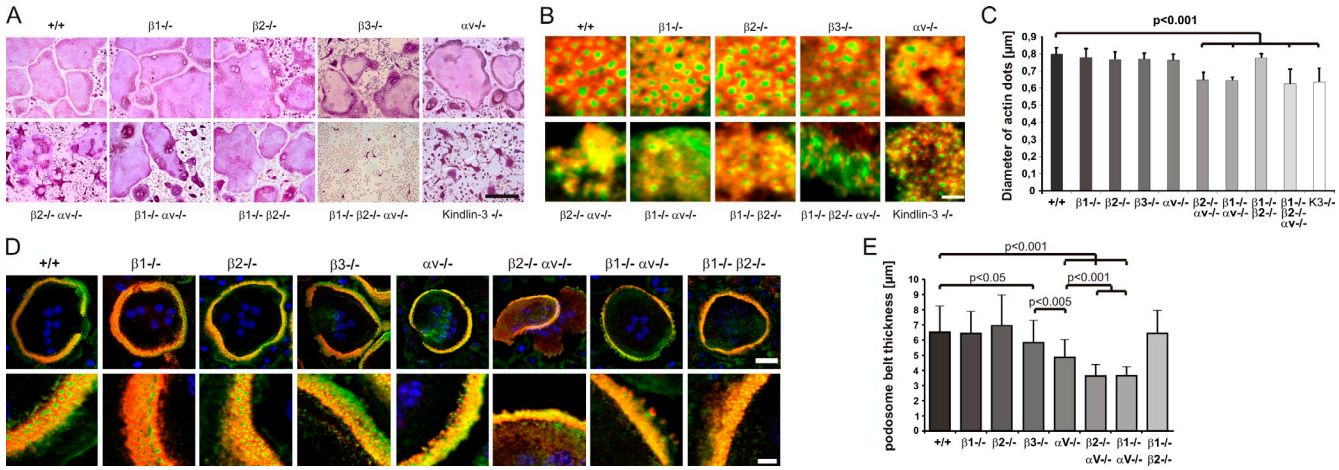

Figure 9. **Podosomes and actin belts in integrin-deficient osteoclasts.** (A) Wild-type and single, double, and triple integrin-deficient osteoclasts stained for TRAP. (B) Vinculin (red) and F-actin staining (phalloidin, green) of wild-type and integrin-deficient pre-osteoclasts plated on glass. (C) Diameters of actin dots in pre-osteoclasts with indicated genotypes measured using MetaMorph software; n = 6/5/5/8/9/6/6/6/8/9 different cells from each genotype taken to measure the actin core size. (D) Vinculin (red) and F-actin staining (phalloidin, green) of wild-type and integrin-deficient osteoclasts plated on glass. DAPI (blue) shows nuclei. (E) Diameter of podosomal belts of wild-type and integrin-deficient osteoclasts plated on glass. Data are presented as mean ± SD (error bars). P-values indicate significant differences from wild-type (Student's t test). Bars: (A) 100 µm; (B) 2 µm; (D, top) 25 µm; (D, bottom) 5 µm.

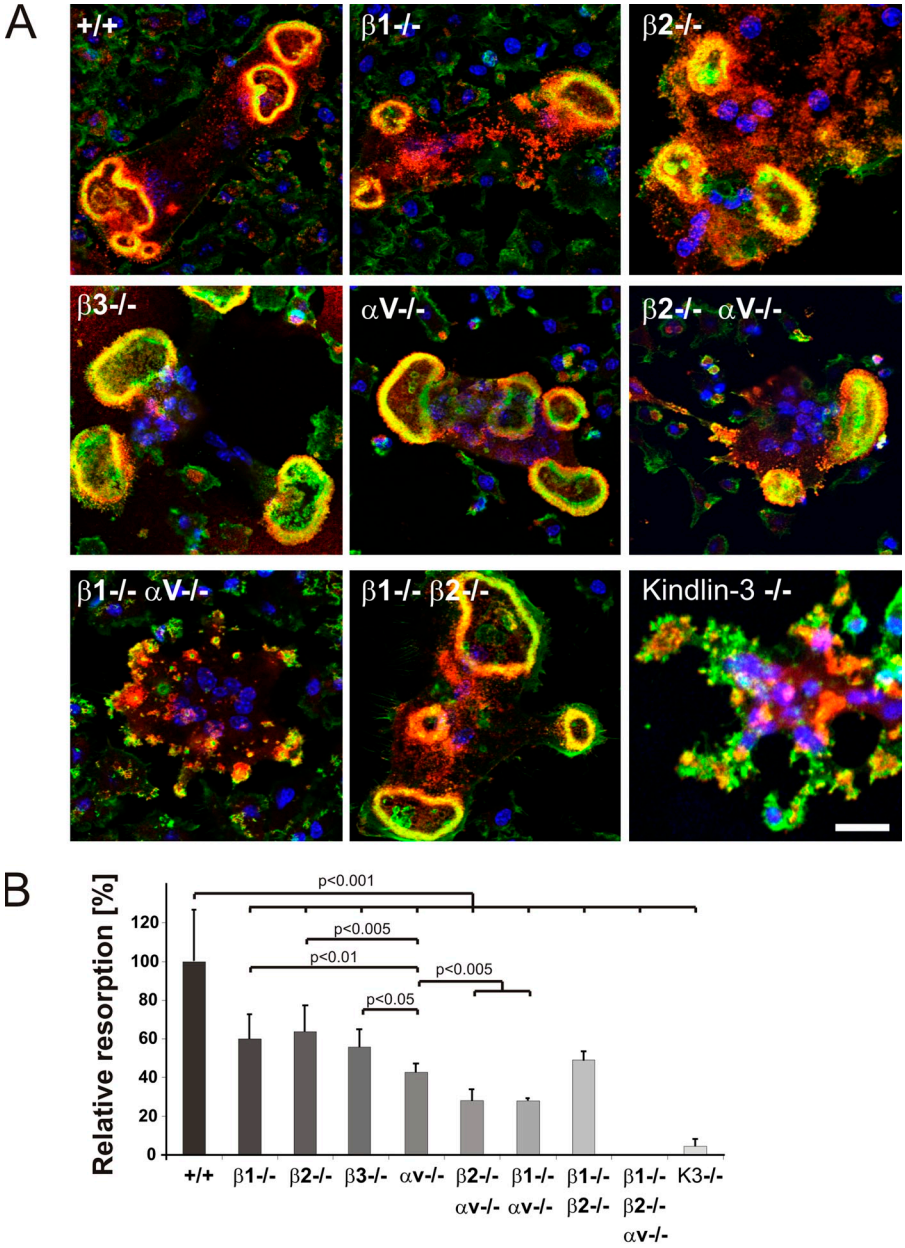

Figure 10. **Sealing zones of integrin-deficient osteoclasts.** (A) Vinculin (red) and F-actin staining (phalloidin, green) of wild-type and integrin-deficient osteoclasts plated on a mineral surface. DAPI staining (blue) shows nuclei. Bar, 25 µm. (B) Resorption activity of wild-type and integrin-deficient osteoclasts plated on calcium apatite-coated slides quantified with MetaMorph. Number of analyzed slides per genotype: n = 26/6/6/6/3/3/3/8. Data are presented as mean ± SD (error bars). P-values indicate significant differences from wild-type (Student's t test).

of osteoclasts, are just one of several integrin players during osteoclast-mediated bone resorption. This finding was corroborated by a series of genetic experiments in which we ablated several integrin genes either individually or in combination in osteoclasts. The experiments revealed an already strongly reduced resorptive activity of osteoclasts when the β1, β2, or αv integrin genes were individually ablated, and a further functional decline when two integrin classes were absent from osteoclasts. The finding that αv-deficient osteoclasts show a significantly more pronounced defect in matrix degradation compared with β3-deficient osteoclasts corroborates our hypothesis that other integrins beside αvβ3 also play an important role in osteoclast function. The ablation of all three integrin classes does not permit osteoclast development in vitro. This made it impossible to test their resorptive activity. In light of the severe defects in osteoclasts lacking two classes of integrins, it is fair to assume that loss of all three integrin classes leads to a further impairment. These findings provide an explanation for the much more severe osteopetrotic phenotype of kindlin-3$^{-/-}$ mice compared with β3 integrin mutants. Interestingly, in contrast to the failure of osteoclast differentiation in the absence of β1, β2, and αv integrins, kindlin-3 deficiency does not impair osteoclast differentiation both in vivo and in vitro. The reason for this observation is not clear. Because kindlins and talins shift the equilibrium of integrins toward their activation state, it is possible that certain processes such as cell fusion can proceed with just a few activated integrins and thus do not require the kindlin-3–mediated equilibrium shift, whereas other processes such as adhesion and podosome formation require a larger number of activated integrins. These questions can be addressed with osteoclasts of engineered mice carrying hypomorphic alleles for β1, β2, and αv integrins. If true, very low levels of integrins

should allow cell fusion but not bone resorption to proceed. An alternative scenario could be that cells that are plated for several days in the presence of serum and integrin ligands can activate integrins from outside and trigger integrin signaling even without efficient inside-out signaling. This is obviously not possible in the absence of all integrin classes.

Loss of kindlin-3 expression or a triple knockout of the β1, β2, and αv integrin genes is also accompanied by impaired podosome formation. Podosomes consist of an integrin ring and a central actin core. Interestingly, small actin cores containing core proteins such as cortactin, Arp2/3, and WASp form in kindlin-3–deficient osteoclasts. Similarly, β1/β2/αv-integrin deficient macrophages also form actin cores with a reduced diameter, indicating that the induction of actin polymerization occurs independently of integrin action, whereas their maturation requires an integrin signaling program. This observation is in agreement with previous studies showing that actin core formation and osteoclast adhesion to the substratum can also be mediated by the transmembrane proteoglycan CD44 in an integrin-independent manner (Chabadel et al., 2007). Actin cores lacking an adhesion ring are also found in c-src–deficient osteoclasts, which suggests that c-src activity is central for their maturation and acts as an upstream signaling molecule required for the assembly of integrins and cytoplasmic adhesion proteins (Destaing et al., 2008; Saltel et al., 2008).

Treatment of kindlin-3$^{-/-}$ osteoclasts with Mn^{2+} significantly improved integrin-mediated adhesion but restored neither the defective F-actin reorganization nor podosome organization and assembly. This finding is in agreement with several reports demonstrating that kindlins mediate both inside-out as well as outside-in integrin signaling (Larjava et al., 2008; Moser et al., 2009b; Plow et al., 2009). Moreover, this interesting observation also indicates that integrin arrangement around F-actin cores cannot be accomplished solely by an active integrin; kindlin-3 and/or kindlin-3–associated proteins are required in addition. Another consequence of the abrogated integrin outside-in signaling in kindlin-3$^{-/-}$ osteoclasts includes diminished FAK and Syk activation upon adhesion to extracellular matrix and impaired Erk and Akt phosphorylation that is seen only upon treatment with low concentrations of M-CSF, whereas high M-CSF levels are associated with normal Erk and Akt phosphorylation, indicating that integrin outside-in signals represent an amplifier of M-CSF–induced c-Fms signaling.

This study shows for the first time that osteoclast-mediated bone resorption depends on multiple integrin classes, which are under control of kindlin-3. Further work will be required to elucidate the individual contributions of each integrin subclass during podosome maturation and assembly, and whether certain signaling pathways that control the organization of the cytoskeleton and the formation of sealing zones are directed by specific integrins in osteoclasts.

Materials and methods

Reagents

Recombinant murine M-CSF and receptor activator of NF-κB ligand (RANKL) were obtained from R&D Systems and PeproTech, respectively. Osteopontin was purified from bovine plasma (provided by D. Heinegard, University of Lund, Lund, Sweden; Franzén and Heinegård, 1985).

Mice

Kindlin-3$^{-/-}$ and integrin β3$^{-/-}$ mice have been described previously (Hodivala-Dilke et al., 1999; Moser et al., 2008). Multiple integrins were deleted by intercrossing mice carrying conditional null mutations in the αv ($\alpha v^{flox/flox}$) and β1 ($\beta 1^{flox/flox}$) genes (Potocnik et al., 2000), a constitutive null mutation in the β2 (β2$^{-/-}$) gene (Scharffetter-Kochanek et al., 1998), and the Mx1Cre transgene (Kühn et al., 1995). All mice were from a mixed 129/SvJxC57BL/6 background. Cre expression in the hematopoietic system was induced by a single intraperitoneal injection of 250 mg polyI/C (GE Healthcare). 7 d after polyI/C treatment, bone marrow cells were isolated and checked for integrin surface expression via FACS. All animals were kept under specific pathogen-free conditions at the animal facility of the Max Planck Institute of Biochemistry.

Antibodies

The following antibodies were used for immunostaining of cells: mouse anti-vinculin antibody, mouse anti-talin, mouse anti-cortactin, rabbit anti-actin, and mouse anti-acetylated tubulin (all from Sigma-Aldrich); rat anti-tubulin, rat anti-integrin β1, and rat anti-integrin αv (all from Millipore); mouse anti–p-Tyrosine (clone pY99) and mouse anti-WASp (both from Santa Cruz Biotechnology, Inc.); rabbit anti-p16 subunit of Arp2/3 complex (Abcam); and FITC and Cy3-labeled secondary antibodies (Jackson ImmunoResearch Laboratories, Inc.). Phalloidin dyes were obtained from Invitrogen.

The following antibodies were used for flow cytometry: hamster IgG anti-integrin β1, isotype control hamster IgG, and isotype control mouse IgG1 (all from Biolegend); rat IgG2a anti-integrin β2, rat IgG2a anti-integrin β7, rat IgG2a anti-integrin α4, rat IgG2a anti-integrin α5, rat IgG2a anti-integrin αL, rat IgG1 anti-integrin αv, isotype control rat IgG1, isotype control rat IgG2a, and rat anti-integrin β1 clone 9EG7 (all from BD); and hamster IgG anti-integrin β3, mouse IgG1 anti-integrin β5, and rat IgG2b anti-integrin αM, isotype control rat IgG2b (all from eBioscience).

The following antibodies were used for Western blotting: mouse anti–glyceraldehyde 3-phosphate dehydrogenase (anti-GAPDH; Merck); rabbit anti-actin and mouse anti-talin (both from Sigma-Aldrich); rabbit anti-JNK, rabbit anti-pJNK Thr183/Tyr185, rabbit anti-p38, rabbit anti-pp38 Thr180/Tyr182, rabbit anti-pSrc Tyr418, rabbit anti-Pyk2, rabbit anti-pPyk2 Tyr402, rabbit anti-P42/44 MAPK, rabbit anti-pP42/44 MAPK Thr202/Tyr204, rabbit anti-Akt, and rabbit anti-pAkt Ser473 (all from Cell Signaling Technology); rabbit anti-FAK and rat anti-tubulin (both from Millipore); rabbit anti-pFAK Tyr397 and rabbit anti-src (both from Invitrogen); and mouse anti-Syk (Abcam).

Histology

Long bones were dissected, freed from soft tissue, and either embedded in plastic (Osteo-Bed Bone Embedding kit, Polysciences Inc.) or decalcified in 10% EDTA/PBS and embedded in paraffin. Paraffin sections were stained with hematoxylin and eosin and for TRAP activity using a commercial kit (Sigma-Aldrich). AP and van Kossa staining were performed according to standard protocols. The number of nuclei in osteoclasts was determined in plastic embedded bone sections from three different 4-d-old animals.

Pictures were taken by bright field microscopy with a microscope (Axioskop; Carl Zeiss, Inc.) equipped with a camera (DC500; Leica), 10× NA 0.3, 20× NA 0.50, and 40× NQ 0.75 objectives, and IM50 software. Pictures were edited with Photoshop (Adobe).

Measurement of RANKL, OPG, and PTH concentrations

Blood was collected from P2–P5 mice after decapitation using a microvette (CB 300 LH; Sarstedt); samples were then centrifuged for 3 min at 7,000 *g* and the plasma was harvested. The concentrations of RANKL and OPG were determined with ELISA kits from R&D Systems, and the intact PTH concentration was determined with an ELISA kit from Immutopics International.

Osteoclast culture

Osteoclasts were differentiated in vitro either from fetal liver cells or from bone marrow. E14.5 wild-type and kindlin-3$^{-/-}$ fetal liver cells were obtained by pushing the fetal liver through a 70-µm cell strainer (BD). The cells were kept in α-MEM supplemented with 20 ng/ml M-CSF overnight (ON). Nonadherent cells were collected after 24 h. Leukocytes were isolated from the interface after centrifugation at 1,000 *g* for 20 min in leukocyte separation medium (Laboratoires Eurobio), then washed with α-MEM medium and seeded at a concentration of 2,000 cells/mm^2 in osteoclast differentiation medium (α-MEM containing 10% heat inactivated FCS, 100 U/ml penicillin, and 100 µg/ml streptomycin with 50 ng/ml M-CSF and 40 ng/ml RANKL). Cells were cultured at 37°C in 5% CO_2 for 5–8 d, and medium was changed every second day. Staining for TRAP

activity was performed after 5 d in culture. Pictures were taken with a microscope (Axioskop) using a 20× NA 0.50 objective (see Histology).

For pre-osteoclast generation, 5×10^6 interface cells were plated on a 10-cm dish and cultured in osteoclast differentiation medium for 2 d. Cells were washed with PBS and lifted with 10 mM EDTA in PBS. Adherent cells that were treated with osteoclast differentiation medium for at least 2 d but had yet not fused into polykaryons were defined as pre-osteoclasts.

Isolation and functional assays with primary osteoblasts

Mouse calvarial osteoblasts were isolated from newborn mice as described previously (Wu et al., 1992). 8×10^4 primary osteoblasts were cultured in α-MEM in a 12-well plate until confluence. Osteoblastogenic medium (α-MEM, 10% FCS, 5 mM β-glycerophosphate, and 10 mg/ml ascorbic acid) was added to induce osteoblast differentiation. Osteoblast identity was confirmed at day 4 of differentiation by RT-PCR for AP, osteocalcin, and collagen I expression.

AP staining was performed on osteoblasts fixed in 4% PFA for 15 min and stained with DIG III solution (0.4% nitro-blue tetrazolium chloride [NBT]/5-bromo-4-chloro-3′-indolyphosphate p-toluidine salt [BCIP], 0.4 M Tris-HCl, pH 9.5, 0.4 M NaCl, and 0.2 M $MgCl_2$). To determine AP activity, osteoblasts from 12-well plates were collected in 500 µl lysis buffer (10 mM Tris-HCl, pH 7.5, 0.5 mM $MgCl_2$, 0.1% Triton X-100, and 1× protease inhibitors) and homogenized by sonication for 20 s followed by centrifugation. 50 µl of the supernatant was mixed with 50 µl of 10 mM p-nitrophenylphosphate (Sigma-Aldrich) in 0.1 M glycine, 1 mM $MgCl_2$, and 1 mM $ZnCl_2$, pH 10.4, and incubated for 30 min at 37°C. 50 µl 1 M NaOH was added to stop the reaction, and absorption at 405 nm was measured. Assays were performed in triplicate and the AP activity was normalized to the initial protein content.

Alizarin red S (ARS) staining and quantification of in vitro mineralization of osteoblasts was performed at day 21 after induction of osteoblast differentiation as described previously (Gregory et al., 2004). In brief, cells were fixed in 4% PFA for 15 min at RT, washed twice with ddH_2O, and incubated with 2% ARS, pH 4.2 (adjusted with NH_4OH) for 20 min while shaking. Cells were washed five times with ddH_2O for 5 min each and pictured. Bound ARS was dissolved in 10% acetic acid for 30 min at RT. The cell layer was scraped from the plate, transferred to a reaction tube, and vigorously shaken for 30 s. The suspension was overlayed with mineral oil, heated to exactly 85°C for 10 min, and kept on ice for 5 min. After centrifugation at 20,000 *g* for 15 min, two equivalents of 10% NH_4OH were added to five equivalents of ARS solution to get a pH of 4.1–4.5. This solution was measured at 405 nm in triplicate.

Pictures were obtained using a stereomicroscope (MZ FLIII; Leica) equipped with a Plan-Apochromat 1.0× objective, a ProgRes C14 camera, and Photoshop (Adobe) software.

RT-PCR

RT-PCR was used to examine the expression levels of osteoclast and osteoblast marker genes. Osteoclasts were obtained as described; cells at time point day 0 were taken immediately after performing the gradient centrifugation, cells at time point day 1 were cultured for 24 h in differentiation medium containing RANKL and M-CSF, and so on.

Total RNA was isolated using an RNeasy kit (QIAGEN). cDNA was obtained using the SuperScriptTM III Reverse transcription kit (Invitrogen). The following primers were used: calcitonin receptor 1b forward, 5′-TTTACCGACGAGCAACGCCTACGC-3′, and reverse, 5′-CATGTAGGACTCGGCCTCGTGGG-3′; cathepsin K forward, 5′-GCTATATGACCACTGCTTTCCAATACG-3′, and reverse, 5′-ACTGCATGGTTCACATTATCACGGTC-3′; GAPDH forward, 5′-TCGTGGATCTGACGTGCCGCCTG-3′, and reverse, 5′-CACCACCCTGTTGCTGTAGCCGT-3′; collagenI forward, 5′-AAGAGGCGAGAGAGGTTTCC-3′, and reverse, 5′-ATCACCAGGTTCACCTTTCG-3′; kindlin-3 forward, 5′-AGCTGTCTCTGCTGCGTGCTC-3′, and reverse, 5′-ATACCTTGCTGCATGAGGCAC-3′; MMP9 forward, 5′-CGAGTGGACGCGACCGTAGTTGG-3′, and reverse, 5′-CAGGCTTAGAGCCACGACCATACAG-3′; kindlin-1 forward, 5′-CTACACCTTCTTTGACTTG-3′, and reverse, 5′-AGGGATGTCAGTTATGTC-3′; kindlin-2 forward, 5′-GTACCGAAGTAGACTGCAAGG-3′, and reverse, 5′-CATACGGCATATCAAGTAGGC-3′; AP forward, 5′-CCTTTGTGGCTCTCTCCAAG-3′, and reverse, 5′-CTGGCCTTCTCATCCAGTTC-3′; and osteocalcin forward, 5′-AAGCAGGAGGGCAATAAGGT-3′, and reverse, 5′-AGCTGCTGTGACATCCATAC-3′.

Adhesion assays

12-mm glass slides were coated for 6 h at RT with 5 µg/ml bovine osteopontin in PBS or with 3% BSA. The adhesion assay was performed with osteoclasts, which were directly isolated from long bones as described previously (Flores et al., 1992; Ek-Rylander et al., 1994). In brief, all four legs of newborn wild-type and kindlin-$3^{-/-}$ mice were minced and rotated for 1 h at 37°C in α-MEM containing 10% FCS. Afterward, the freed cells were seeded onto the coated-glass slides for 1 h and the slides were carefully washed with medium to remove nonadherent cells. The adherent cells were allowed to spread ON and were then TRAP-stained.

Macrophage adhesion on ICAM-1 was performed as described previously (Chavakis et al., 2008). In brief, 96-well plates were coated with 4 µg/ml recombinant human ICAM-1 (R&D Systems) in coating buffer (150 mM NaCl, 20 mM Tris-HCl, and 2 mM $MgCl_2$, pH 9) ON at 4°C, blocked with 3% BSA in PBS for 1 h at RT, then incubated with 50,000 macrophages for 30 min in a tissue culture incubator in the presence or absence of 1 mM $MnCl_2$. Each condition was assayed in quadruplet. After washing with PBS containing 1% BSA, adherent cells were fixed in 4% PFA for 10 min and stained with 5 mg/ml crystal violet in 2% ethanol for 30 min. After washing, the remaining dye was dissolved in 2% SDS. Staining intensity was measured in an ELISA plate reader at 550 nm.

Resorption assay

Osteoclasts isolated from bones of P2–P4 wild-type and kindlin-$3^{-/-}$ mice or in vitro differentiated from fetal liver cells or bone marrow were plated in osteoclast differentiation medium on osteologic slides (BD) for 1 wk. To quantify matrix resorption, cells were removed from the slides by treating them with 1% Triton X-100 and mechanical agitation, pictures were obtained with a microscope (Axioskop; 20× NA 0.50 objective, see Histology), and the resorbed area was measured using MetaMorph software. Alternatively, cells were cultured on dentin discs (Immunodiagnostic Systems) and resorption pits were visualized by staining with 1% toluidine blue in 0.5% sodium tetraborate for 3 min.

Immunofluorescence

Cells were plated on 12-mm coverslips coated with FCS for 1 h at 37°C, fixed with 4% PFA in PBS for 10 min or with 4% PFA for 1 min followed by a methanol fixation for 10 min at −20°C, and permeabilized with 0.25% Triton X-100 in PBS for 20 min. Blocking was performed for 1 h with 3% BSA in PBS. Cells were then incubated with the primary antibody in blocking solution for 3 h at RT or at 4°C ON. F-actin was visualized with Alexa Fluor 488–Phalloidin or Alexa Fluor 647–Phalloidin. Cells were imaged at RT with a SP2 confocal microscope (DMIRE2; Leica) using Leica Confocal Software (version 2.5 Build 1227) with 40× NA 1.25 and 100× NA 1.40 oil objective lenses. Single channels were imaged sequentially. All pictures were processed with Photoshop (Adobe).

Actin core size was measured in the actin channel by using MetaMorph software from at least six cells of each genotype. 50 actin dots were measured from each individual cell. The podosome belt size was obtained by measuring the thickness of the vinculin ring of at least 20 belts from osteoclasts that were differentiated in three or more independent preparations. Actin cores from at least 10 different pre-osteoclasts were analyzed. From each cell, 25 actin cores were analyzed.

Retroviral infections

EGFP–kindlin-3 and EGFP–kindlin-3–QA constructs (Moser et al., 2008) were amplified and directionally cloned using the EcoRI and BamHI sites of the pCLMFG retroviral vector (Naviaux et al., 1996). Vesicular stomatitis virus G–pseudotyped retroviral vectors were produced by transient transfection of 293T (human embryonic kidney) cells. Viral particles were concentrated from cell culture supernatant as described previously (Pfeifer et al., 2000) and used for infection of fetal liver cells. Fetal liver cells were prepared for differentiation into osteoclasts as described. Cells were cultured in medium containing 10 ng/ml M-CSF and 40 ng/ml RANKL for 5 d, and were used for TRAP and immunofluorescence staining and matrix degradation assays, or were lysed for Western blotting.

Gelatin zymography

Osteoclasts were isolated from bones of P2–P4 wild-type and kindlin-$3^{-/-}$ mice, plated in osteoclast differentiation medium in a single 24 well for about 1 wk, and washed and incubated with serum-free α-MEM for 24 h. The conditioned medium was harvested, concentrated in Centricon filter units (10 kD cut-off; Millipore), mixed with nonreducing SDS sample buffer, and run on an SDS gel with a 4% stacking gel and a 12% running gel containing 0.2% gelatin. Gels were incubated twice for 15 min at RT in 0.2% Triton X-100 in ddH_2O and then for several days at 37°C in MMP reaction buffer (50 mM Tris-HCl, pH 7.5, 0.2 M NaCl, 5 mM $CaCl_2$, and 0.02% NaN_3). The bands of gelatinolytic activity were revealed after staining with Coomassie blue.

Cathepsin K activity measurement

Functional cathepsin K concentration was measured in protein lysates of cultured osteoclasts using a Cathepsin K Activity Assay kit (BioVision, Inc.). The assay was performed according to the manufacturer's instructions using 50 µg protein lysate per measurement.

Bone mineral density and histomorphometric measurements

pQCT of the distal femur was performed with XCT Research SA+ (StraTec Medizintechnik). Bone density was measured exactly in the middle of the bone length using peel mode 2 with the threshold set at 100. Calcein labeling was performed as follows: 50 µl of 5 mg/ml calcein (Sigma-Aldrich) in 0.9% NaCl and 50 mM $NaHCO_3$ was injected at P0 and exactly 24 h later intraperitoneally. Mice were sacrificed 15 h after the second injection and long bones were dissected, fixed in 70% ethanol, and embedded in polymethylmethacrylate. 3-µm sections of the distal femur were deplasticized and stained for Masson-Goldner with hematoxylin (Gill II; Carl Roth), acid fuchsin-ponceau xylidine, and phosphomolybdic acid-orange G for visualizing cells, and osteoid and light green for visualizing mineralized matrix. Cancellous bone was examined in the 1-mm band below the growth plate, whereas primary cancellous bone was examined in the first 200 µm and secondary cancellous bone in the remaining 800 µm. Data presented were combined for both types. Histomorphometric analysis was performed according to the standards set forth by the American Society for Bone and Mineral Research (Parfitt et al., 1987). The following parameters were examined: osteoid surface (OS), bone surface (BS), osteoblast number (Ob.N), osteoclast number (Oc.N), and osteoclast surface (Oc.S). Measurements were performed by a person blinded to the genotype of the mice.

Flow cytometry

Fetal liver cell–derived macrophages and pre-osteoclasts were incubated with Fc receptor–blocking antibody (Millipore) and then with the appropriate fluorophore-conjugated monoclonal antibodies for 30 min on ice. Analysis was performed with a FACSCalibur (BD). β1 integrin activation was induced with 2 mM Mn^{2+} and analyzed with the 9EG7 antibody and a fluorophore-conjugated anti–rat antibody. 9EG7 binding was normalized to β1 integrin surface levels.

FNIII7-10 binding assay

Human FNIII7-10 fragment was subcloned into pET15b plasmid (Invitrogen), expressed in bacteria, and subsequently labeled with Alexa Fluor 647 carboxylic acid via a succinimidyl ester (Invitrogen) as described previously (Czuchra et al., 2006). To assess ligand-binding properties, fetal liver–derived macrophages were harvested and incubated with Alexa Fluor 647–coupled FNIII7-10 fragment in TBS in the presence or absence of 10 mM EDTA or 2 mM $MnCl_2$, respectively, and then subjected to flow cytometry analysis. Mean fluorescence of EDTA-treated cells was considered unspecific signal and was subtracted from all values.

Blocking of CD44-mediated adhesion

Osteoclast precursors were lifted using 10 mM EDTA in PBS and were first incubated for 15 min with an Fc receptor–blocking antibody followed by a 15 min incubation with either an anti-CD44–blocking antibody (BD) or rat IgG2b (eBioscience) before seeding on a fibronectin-coated surface. After adhesion for 30 min, cells were carefully rinsed with PBS and fixed with 4% PFA. Pictures were obtained using a microscope (Axiovert 40C; Carl Zeiss, Inc.) with a camera (Prosilica), a 10× objective lens, and FireWire Recorder software.

RANKL- and M-CSF-signaling

Mature osteoclasts were serum starved in α-MEM for 3–4 h and treated with either recombinant M-CSF (100 ng/ml or 10 ng/ml) or recombinant RANKL (100 ng/ml) for the times indicated. Cells were washed in cold PBS, lysed on ice with modified RIPA lysis buffer (50 mM Tris-HCl, pH7.3, 150 mM NaCl, 2 mM EDTA, 1% Triton X-100, 0.5% sodium deoxycholate, 1× protease inhibitor mixture [Roche], and 1× phosphatase inhibitor cocktail 1+2 [Sigma-Aldrich]) and incubated on ice for 10 min. Cell lysates were cleared by centrifugation at 14,000 rpm for 10 min at 4°C, and 40 µg of total lysates was subjected to 10% SDS-PAGE, transferred onto polyvinylidene fluoride membranes, blocked for 1 h in 5% BSA in TBS-T for detecting phosphorylated proteins or in 5% skim milk in TBS-T for detecting other proteins, then incubated with primary antibodies at 4°C ON followed by probing with HRP-labeled secondary antibodies (Jackson ImmunoResearch Laboratories).

For detection of Syk phosphorylation, 500 µg of lysate was used for immunoprecipitation. Lysate was incubated with 3 µg of primary antibody ON at 4°C on a rotator, then protein G–Sepharose beads (Sigma-Aldrich) were added to the lysates, incubated for 3 h at 4°C on a rotator, washed three times in lysis buffer, and boiled in 3× SDS sample buffer for 5 min. After centrifugation, proteins were separated by 10% SDS-PAGE, Western blotted, and probed using an HRP-labelled 4G10 antibody (Millipore).

Electron microscopy

Primary osteoclasts were cultured on glass coverslips and then "unroofed" as described previously (Heuser, 2000; Luxenburg et al., 2007). In brief, cells were exposed to hypotonic buffer (20% PHEM, 6 mM Pipes, 5 mM Hepes, 0.4 mM Mg_2SO_4, and 2 mM EGTA) and broken by brief sonication for 2 s. The resulting ventral membrane preparations were fixed with 2.5% (vol/vol) glutaraldehyde in 0.1 M phosphate buffer (pH 7.4, 1 h at RT), postfixed with 1% (wt/vol) aqueous OsO_4, dehydrated, critical-point dried, and sputter-coated with 10 nm Au-Pd. Samples were viewed at 5 kV with a scanning electron microscope (DSM 982-Gemini; Carl Zeiss, Inc.).

Statistical analysis

A Student's *t* test was used to analyze histomorphometric data, osteoblast data, ELISA assays, β1 integrin activation, osteoclast fusion, belt thickness, resorption, and adhesion. $P < 0.05$ was considered to be statistically significant. All graphs include standard deviation error bars.

Online supplemental material

Fig. S1 shows histological sections of control and kindlin-3$^{-/-}$ long bones from different developmental stages indicating progressive ossification in kindlin-3$^{-/-}$ mice. Fig. S2 shows normal biological activity of kindlin-3$^{-/-}$ osteoblasts. Fig. S3 shows normal p38 and JNK phosphorylation of kindlin-3$^{-/-}$ osteoclasts upon RANKL treatment in vitro. Fig. S4 shows that CD44 contributes to the residual adhesion of kindlin-3$^{-/-}$ pre-osteoclasts and integrin surface expression levels on control and kindlin-3$^{-/-}$ macrophages. Fig. S5 shows that retroviral-expressed EGFP–kindlin-3 rescues cell spreading, podosome formation, and matrix degradation in kindlin-3$^{-/-}$ osteoclasts, whereas expression of an integrin-binding mutant EGFP–kindlin-3 construct fails to do so.

We thank the Fässler laboratory members for discussion and Kyle Legate for critically reading the manuscript, Hildegard Reiter for performing the retroviral infections, Dick Heinegard for osteopontin, Angelika Flörl (Innsbruck Medical University, Austria) for excellent technical assistance with the electron microscopy work, and Chantal Domenget (University of Lyon, France) for support with osteoclast culture. We also thank Shahin Begum and Richard Hynes (Massachusetts Institute of Technology, Cambridge, MA) for isolating and providing bones from β3 integrin-deficient mice.

The work was supported by seventh framework program of the European Union and the Max Planck Society. The authors declare that they have no competing financial interests.

Submitted: 26 July 2010
Accepted: 2 February 2011

References

Chabadel, A., I. Bañon-Rodríguez, D. Cluet, B.B. Rudkin, B. Wehrle-Haller, E. Genot, P. Jurdic, I.M. Anton, and F. Saltel. 2007. CD44 and beta3 integrin organize two functionally distinct actin-based domains in osteoclasts. *Mol. Biol. Cell.* 18:4899–4910. doi:10.1091/mbc.E07-04-0378

Chavakis, E., G. Carmona, C. Urbich, S. Göttig, R. Henschler, J.M. Penninger, A.M. Zeiher, T. Chavakis, and S. Dimmeler. 2008. Phosphatidylinositol-3-kinase-gamma is integral to homing functions of progenitor cells. *Circ. Res.* 102:942–949. doi:10.1161/CIRCRESAHA.107.164376

Czuchra, A., H. Meyer, K.R. Legate, C. Brakebusch, and R. Fässler. 2006. Genetic analysis of beta1 integrin "activation motifs" in mice. *J. Cell Biol.* 174:889–899. doi:10.1083/jcb.200604060

Destaing, O., F. Saltel, J.C. Géminard, P. Jurdic, and F. Bard. 2003. Podosomes display actin turnover and dynamic self-organization in osteoclasts expressing actin-green fluorescent protein. *Mol. Biol. Cell.* 14:407–416. doi:10.1091/mbc.E02-07-0389

Destaing, O., F. Saltel, B. Gilquin, A. Chabadel, S. Khochbin, S. Ory, and P. Jurdic. 2005. A novel Rho-mDia2-HDAC6 pathway controls podosome patterning through microtubule acetylation in osteoclasts. *J. Cell Sci.* 118:2901–2911. doi:10.1242/jcs.02425

Destaing, O., A. Sanjay, C. Itzstein, W.C. Horne, D. Toomre, P. De Camilli, and R. Baron. 2008. The tyrosine kinase activity of c-Src regulates actin dynamics and organization of podosomes in osteoclasts. *Mol. Biol. Cell.* 19:394–404. doi:10.1091/mbc.E07-03-0227

Ek-Rylander, B., M. Flores, M. Wendel, D. Heinegård, and G. Andersson. 1994. Dephosphorylation of osteopontin and bone sialoprotein by osteoclastic tartrate-resistant acid phosphatase. Modulation of osteoclast adhesion in vitro. *J. Biol. Chem.* 269:14853–14856.

Faccio, R., D.V. Novack, A. Zallone, F.P. Ross, and S.L. Teitelbaum. 2003a. Dynamic changes in the osteoclast cytoskeleton in response to growth factors and cell attachment are controlled by beta3 integrin. *J. Cell Biol.* 162:499–509. doi:10.1083/jcb.200212082

Faccio, R., S. Takeshita, A. Zallone, F.P. Ross, and S.L. Teitelbaum. 2003b. c-Fms and the alphavbeta3 integrin collaborate during osteoclast differentiation. *J. Clin. Invest.* 111:749–758.

Flores, M.E., M. Norgård, D. Heinegård, F.P. Reinholt, and G. Andersson. 1992. RGD-directed attachment of isolated rat osteoclasts to osteopontin, bone sialoprotein, and fibronectin. *Exp. Cell Res.* 201:526–530. doi:10.1016/0014-4827(92)90305-R

Franzén, A., and D. Heinegård. 1985. Isolation and characterization of two sialoproteins present only in bone calcified matrix. *Biochem. J.* 232:715–724.

Gil-Henn, H., O. Destaing, N.A. Sims, K. Aoki, N. Alles, L. Neff, A. Sanjay, A. Bruzzaniti, P. De Camilli, R. Baron, and J. Schlessinger. 2007. Defective microtubule-dependent podosome organization in osteoclasts leads to increased bone density in Pyk2(-/-) mice. *J. Cell Biol.* 178:1053–1064. doi:10.1083/jcb.200701148

Goodison, S., V. Urquidi, and D. Tarin. 1999. CD44 cell adhesion molecules. *MP, Mol. Pathol.* 52:189–196. doi:10.1136/mp.52.4.189

Grant, F.D., P.R. Conlin, and E.M. Brown. 1990. Rate and concentration dependence of parathyroid hormone dynamics during stepwise changes in serum ionized calcium in normal humans. *J. Clin. Endocrinol. Metab.* 71:370–378. doi:10.1210/jcem-71-2-370

Gregory, C.A., W.G. Gunn, A. Peister, and D.J. Prockop. 2004. An Alizarin red-based assay of mineralization by adherent cells in culture: comparison with cetylpyridinium chloride extraction. *Anal. Biochem.* 329:77–84. doi:10.1016/j.ab.2004.02.002

Helfrich, M.H., S.A. Nesbitt, P.T. Lakkakorpi, M.J. Barnes, S.C. Bodary, G. Shankar, W.T. Mason, D.L. Mendrick, H.K. Väänänen, and M.A. Horton. 1996. Beta 1 integrins and osteoclast function: involvement in collagen recognition and bone resorption. *Bone*. 19:317–328. doi:10.1016/S8756-3282(96)00223-2

Heuser, J. 2000. The production of 'cell cortices' for light and electron microscopy. *Traffic*. 1:545–552. doi:10.1034/j.1600-0854.2000.010704.x

Hodivala-Dilke, K.M., K.P. McHugh, D.A. Tsakiris, H. Rayburn, D. Crowley, M. Ullman-Culleré, F.P. Ross, B.S. Coller, S. Teitelbaum, and R.O. Hynes. 1999. Beta3-integrin-deficient mice are a model for Glanzmann thrombasthenia showing placental defects and reduced survival. *J. Clin. Invest.* 103:229–238. doi:10.1172/JCI5487

Jurdic, P., F. Saltel, A. Chabadel, and O. Destaing. 2006. Podosome and sealing zone: specificity of the osteoclast model. *Eur. J. Cell Biol.* 85:195–202. doi:10.1016/j.ejcb.2005.09.008

Kilic, S.S., and A. Etzioni. 2009. The clinical spectrum of leukocyte adhesion deficiency (LAD) III due to defective CalDAG-GEF1. *J. Clin. Immunol.* 29:117–122. doi:10.1007/s10875-008-9226-z

Krüger, M., M. Moser, S. Ussar, I. Thievessen, C.A. Luber, F. Forner, S. Schmidt, S. Zanivan, R. Fässler, and M. Mann. 2008. SILAC mouse for quantitative proteomics uncovers kindlin-3 as an essential factor for red blood cell function. *Cell*. 134:353–364. doi:10.1016/j.cell.2008.05.033

Kühn, R., F. Schwenk, M. Aguet, and K. Rajewsky. 1995. Inducible gene targeting in mice. *Science*. 269:1427–1429. doi:10.1126/science.7660125

Kuijpers, T.W., E. van de Vijver, M.A. Weterman, M. de Boer, A.T. Tool, T.K. van den Berg, M. Moser, M.E. Jakobs, K. Seeger, O. Sanal, et al. 2009. LAD-1/variant syndrome is caused by mutations in FERMT3. *Blood*. 113:4740–4746. doi:10.1182/blood-2008-10-182154

Larjava, H., E.F. Plow, and C. Wu. 2008. Kindlins: essential regulators of integrin signalling and cell-matrix adhesion. *EMBO Rep.* 9:1203–1208. doi:10.1038/embor.2008.202

Legate, K.R., S.A. Wickström, and R. Fässler. 2009. Genetic and cell biological analysis of integrin outside-in signaling. *Genes Dev.* 23:397–418. doi:10.1101/gad.1758709

Linder, S., and M. Aepfelbacher. 2003. Podosomes: adhesion hot-spots of invasive cells. *Trends Cell Biol.* 13:376–385. doi:10.1016/S0962-8924(03)00128-4

Linder, S., and P. Kopp. 2005. Podosomes at a glance. *J. Cell Sci.* 118:2079–2082. doi:10.1242/jcs.02390

Luxenburg, C., D. Geblinger, E. Klein, K. Anderson, D. Hanein, B. Geiger, and L. Addadi. 2007. The architecture of the adhesive apparatus of cultured osteoclasts: from podosome formation to sealing zone assembly. *PLoS ONE*. 2:e179. doi:10.1371/journal.pone.0000179

Malinin, N.L., L. Zhang, J. Choi, A. Ciocea, O. Razorenova, Y.Q. Ma, E.A. Podrez, M. Tosi, D.P. Lennon, A.I. Caplan, et al. 2009. A point mutation in KINDLIN3 ablates activation of three integrin subfamilies in humans. *Nat. Med.* 15:313–318. doi:10.1038/nm.1917

McDowall, A., L. Svensson, P. Stanley, I. Patzak, P. Chakravarty, K. Howarth, H. Sabnis, M. Briones, and N. Hogg. 2010. Two mutations in the KINDLIN3 gene of a new leukocyte adhesion deficiency III patient reveal distinct effects on leukocyte function in vitro. *Blood*. 115:4834–4842. doi:10.1182/blood-2009-08-238709

McHugh, K.P., K. Hodivala-Dilke, M.H. Zheng, N. Namba, J. Lam, D. Novack, X. Feng, F.P. Ross, R.O. Hynes, and S.L. Teitelbaum. 2000. Mice lacking beta3 integrins are osteosclerotic because of dysfunctional osteoclasts. *J. Clin. Invest.* 105:433–440. doi:10.1172/JCI8905

Moser, M., B. Nieswandt, S. Ussar, M. Pozgajova, and R. Fässler. 2008. Kindlin-3 is essential for integrin activation and platelet aggregation. *Nat. Med.* 14:325–330. doi:10.1038/nm1722

Moser, M., M. Bauer, S. Schmid, R. Ruppert, S. Schmidt, M. Sixt, H.V. Wang, M. Sperandio, and R. Fässler. 2009a. Kindlin-3 is required for beta2 integrin-mediated leukocyte adhesion to endothelial cells. *Nat. Med.* 15:300–305. doi:10.1038/nm.1921

Moser, M., K.R. Legate, R. Zent, and R. Fässler. 2009b. The tail of integrins, talin, and kindlins. *Science*. 324:895–899. doi:10.1126/science.1163865

Naviaux, R.K., E. Costanzi, M. Haas, and I.M. Verma. 1996. The pCL vector system: rapid production of helper-free, high-titer, recombinant retroviruses. *J. Virol.* 70:5701–5705.

Parfitt, A.M., M.K. Drezner, F.H. Glorieux, J.A. Kanis, H. Malluche, P.J. Meunier, S.M. Ott, and R.R. Recker. 1987. Bone histomorphometry: standardization of nomenclature, symbols, and units. *J. Bone Miner. Res.* 2:595–610. doi:10.1002/jbmr.5650020617

Pfeifer, A., T. Kessler, S. Silletti, D.A. Cheresh, and I.M. Verma. 2000. Suppression of angiogenesis by lentiviral delivery of PEX, a noncatalytic fragment of matrix metalloproteinase 2. *Proc. Natl. Acad. Sci. USA*. 97:12227–12232. doi:10.1073/pnas.220399597

Plow, E.F., J. Qin, and T. Byzova. 2009. Kindling the flame of integrin activation and function with kindlins. *Curr. Opin. Hematol.* 16:323–328. doi:10.1097/MOH.0b013e32832ea389

Ponta, H., L. Sherman, and P.A. Herrlich. 2003. CD44: from adhesion molecules to signalling regulators. *Nat. Rev. Mol. Cell Biol.* 4:33–45. doi:10.1038/nrm1004

Potocnik, A.J., C. Brakebusch, and R. Fässler. 2000. Fetal and adult hematopoietic stem cells require beta1 integrin function for colonizing fetal liver, spleen, and bone marrow. *Immunity*. 12:653–663. doi:10.1016/S1074-7613(00)80216-2

Rao, H., G. Lu, H. Kajiya, V. Garcia-Palacios, N. Kurihara, J. Anderson, K. Patrene, D. Sheppard, H.C. Blair, J.J. Windle, et al. 2006. Alpha9beta1: a novel osteoclast integrin that regulates osteoclast formation and function. *J. Bone Miner. Res.* 21:1657–1665. doi:10.1359/jbmr.060718

Ross, F.P., and S.L. Teitelbaum. 2005. alphavbeta3 and macrophage colony-stimulating factor: partners in osteoclast biology. *Immunol. Rev.* 208:88–105. doi:10.1111/j.0105-2896.2005.00331.x

Sabnis, H., A. Kirpalani, J. Horan, A. McDowall, L. Svensson, A. Cooley, T. Merck, S. Jobe, N. Hogg, and M. Briones. 2010. Leukocyte adhesion deficiency-III in an African-American patient. *Pediatr. Blood Cancer*. 55:180–182.

Saltel, F., A. Chabadel, E. Bonnelye, and P. Jurdic. 2008. Actin cytoskeletal organisation in osteoclasts: a model to decipher transmigration and matrix degradation. *Eur. J. Cell Biol.* 87:459–468. doi:10.1016/j.ejcb.2008.01.001

Scharffetter-Kochanek, K., H. Lu, K. Norman, N. van Nood, F. Munoz, S. Grabbe, M. McArthur, I. Lorenzo, S. Kaplan, K. Ley, et al. 1998. Spontaneous skin ulceration and defective T cell function in CD18 null mice. *J. Exp. Med.* 188:119–131. doi:10.1084/jem.188.1.119

Suda, T., N. Takahashi, N. Udagawa, E. Jimi, M.T. Gillespie, and T.J. Martin. 1999. Modulation of osteoclast differentiation and function by the new members of the tumor necrosis factor receptor and ligand families. *Endocr. Rev.* 20:345–357. doi:10.1210/er.20.3.345

Svensson, L., K. Howarth, A. McDowall, I. Patzak, R. Evans, S. Ussar, M. Moser, A. Metin, M. Fried, I. Tomlinson, and N. Hogg. 2009. Leukocyte adhesion deficiency-III is caused by mutations in KINDLIN3 affecting integrin activation. *Nat. Med.* 15:306–312. doi:10.1038/nm.1931

Teitelbaum, S.L., and F.P. Ross. 2003. Genetic regulation of osteoclast development and function. *Nat. Rev. Genet.* 4:638–649. doi:10.1038/nrg1122

Ussar, S., H.V. Wang, S. Linder, R. Fässler, and M. Moser. 2006. The Kindlins: subcellular localization and expression during murine development. *Exp. Cell Res.* 312:3142–3151. doi:10.1016/j.yexcr.2006.06.030

Weinstein, E.J., M. Bourner, R. Head, H. Zakeri, C. Bauer, and R. Mazzarella. 2003. URP1: a member of a novel family of PH and FERM domain-containing membrane-associated proteins is significantly over-expressed in lung and colon carcinomas. *Biochim. Biophys. Acta*. 1637:207–216.

Wu, H., R. Fässler, A. Schnieke, D. Barker, K.H. Lee, V. Chapman, U. Francke, and R. Jaenisch. 1992. An X-linked human collagen transgene escapes X inactivation in a subset of cells. *Development*. 116:687–695.